Downloaded from rsta.royalsocietypublishing.org

PHILOSOPHICAL TRANSACTIONS OF THE ROYAL SOCIETY A MATHEMATICAL, PHYSICAL & ENGINEERING SCIENCES

An examination of simulated geomagnetic reversals from a palaeomagnetic perspective

Robert S. Coe, Lionel Hongre and Gary A. Glatzmaier

Phil. Trans. R. Soc. Lond. A 2000 **358**, 1141-1170
doi: 10.1098/rsta.2000.0578

Email alerting service

Receive free email alerts when new articles cite this article - sign up in the box at the top right-hand corner of the article or click **here**

To subscribe to *Phil. Trans. R. Soc. Lond. A* go to:
http://rsta.royalsocietypublishing.org/subscriptions

This journal is © 2000 The Royal Society

Downloaded from rsta.royalsocietypublishing.org

THE ROYAL SOCIETY

An examination of simulated geomagnetic reversals from a palaeomagnetic perspective

By Robert S. Coe, Lionel Hongre and Gary A. Glatzmaier

Department of Earth Sciences, University of California, Santa Cruz, CA 95064, USA

Four magnetic polarity reversals that occurred during two numerical simulations of the Glatzmaier–Roberts geodynamo display a range of behaviour that resembles records of real reversals of the Earth's magnetic field in some ways, and suggests additional insights in others. Two reversals happened during the homogeneous simulation, which prescribes spatially uniform heat flux at the core–mantle boundary (CMB); and two occurred during the tomographic simulation, which specifies variable CMB heat flux patterned after a low-order seismic velocity model from tomographic investigation of the lower mantle. All but one were accomplished within 2000–7000 (model) years, whereas the second tomographic reversal took 22 000 years. The two homogeneous transitions display low intensities typical of real reversals, with longer-term variation resembling what has been called 'sawtooth' behaviour. During the first tomographic reversal extremely high non-dipole fields occur in some regions, the result of strong patches of vertical flux that appear in less than 100 years and grow rapidly for several hundred more. The intensity during the second tomographic reversal is unusually low for a long time, and large-amplitude oscillations in direction are common. The fields in the middle of the polarity transitions are dominantly non-dipolar for all but the first tomographic reversal. One consists of spherical harmonics that are mainly antisymmetric about the equator, two by symmetric harmonics, and one by a mixture of symmetric and antisymmetric harmonics. Despite this wide variety of characteristics, all reversals occur when the non-dipole energy trend is upward. Finally, after running 300 kyr and reversing twice, the density of transitional virtual geomagnetic poles in the tomographic simulations exhibits a crude statistical correlation with areas of higher-than-average CMB heat flux, offering some support for hypotheses of preferred bands and patches.

Keywords: geomagnetic reversals; polarity transitions; geodynamo simulations; palaeomagnetism; core processes; geomagnetism

1. Introduction

During the past 25 years, the palaeomagnetic community has invested substantial effort in obtaining records of geomagnetic polarity reversals. Although these demonstrate that there is significant variation in the detailed field behaviour for different reversals and at different places during the same reversal, there are broad similarities among many reversal records (Bogue & Merrill 1992; Hoffman 1992, 1996; Jacobs 1994). The average duration for field reversal is *ca.* 5 kyr and the transition field

© 2000 The Royal Society

Downloaded from rsta.royalsocietypublishing.org

PHILOSOPHICAL TRANSACTIONS OF THE ROYAL SOCIETY A MATHEMATICAL, PHYSICAL & ENGINEERING SCIENCES

intensity is usually lower by 50–90% when directions are intermediate between normal and reversed polarity. Before attaining stable polarity of the opposite sense, the direction during the transition may briefly rebound to its old polarity; or it may continue on to new polarity while regaining much or all of the intensity it lost, only to revert shortly thereafter to intermediate directions and low intensities before finally achieving stable reversal. In addition, some of the most detailed studies in lava flows and sediments suggest that

(i) the transitional field may linger around some 'preferred' direction and move rapidly away from others (Mankinen *et al*. 1985; Hoffman 1992, 1996; Glen *et al*. 1994);

(ii) the field intensity before or just after completion of the reversal may temporarily overshoot the ordinary value for full polarity by 50% or more (Prévot *et al*. 1985*a*, *b*; Bogue & Merrill 1992); and

(iii) the behaviour of the fields in successive reversals at a given location is sometimes much more similar than would be expected by coincidence (Bogue & Coe 1982; Clement *et al*. 1995; Herrero-Bervera & Coe 1999).

Nonetheless, because of the scarcity of such records and their limitations as regards completeness, resolution and fidelity, many questions still remain about the character of reversals. For example, is the field predominantly dipolar or non-dipolar when it is reversing? Early evidence for low intensity during reversals convinced most scientists that the transition field is mainly non-dipolar, the dipole field decaying away and then growing back with opposite sign (Van Zijl *et al*. 1962; Momose 1963). A few scientists, however, favoured inclined dipole explanations for the intermediate directions (Creer & Ispir 1970; Steinhauser & Vincenz 1973). When Hillhouse & Cox (1976) published their Western US Lake Tecopa record of the Matuyama–Brunhes reversal, showing that the virtual geomagnetic poles (VGPs) fell in a very different longitudinal band from that defined by VGPs from the Japanese Boso Peninsula record (Niitsuma 1971) of the same reversal, the non-dipolar hypothesis appeared to be confirmed and the question settled. This satisfying state of affairs did not last for long, though: Valet *et al*. (1988) restudied the Lake Tecopa sediments and found quite different VGPs that depended on the type of laboratory demagnetization employed, suggesting that the rocks had acquired a secondary chemical remanence and that the transition record was not reliable.

The debate has continued without resolution, even as more records from both sedimentary and volcanic rocks have accumulated. Some authors cite records that show clustering of transitional VGPs of records into preferred longitudinal bands (Laj *et al*. 1991) or patches (Hoffman 1992) as evidence for dipole predominance (Tric *et al*. 1991; Clement 1992; Hoffman 1996). Others have contested the reality of such geographical clustering for a variety of reasons (Rochette 1990; Langereis *et al*. 1992; Valet *et al*. 1992; McFadden *et al*. 1993; Prévot & Camps 1993; Quidelleur & Valet 1994; Quidelleur *et al*. 1995). We return to this question toward the end of the paper when we examine the simulations for geographic confinement.

The question of whether transitional VGPs cluster geographically raises another important issue more directly: to what extent do lateral inhomogeneities in the lowermost mantle exert control on the course of reversal? The preferred bands and patches that have been proposed lie above lower-mantle regions inferred to have relatively

Downloaded from rsta.royalsocietypublishing.org

PHILOSOPHICAL TRANSACTIONS OF THE ROYAL SOCIETY A MATHEMATICAL, PHYSICAL & ENGINEERING SCIENCES

high seismic velocity (Su *et al*. 1994), which indicates lower-than-average temperature, different chemical composition, or both. Many authors have pointed out that lateral variations in temperature gradient at the core–mantle boundary (CMB) would cause proportional variations in the heat conducted across it. This would presumably affect dynamo processes in the core (Cox & Doell 1964; Hide 1970; Bloxham & Gubbins 1987), and it might produce clustering of transitional VGPs. If such were in fact the case for the Earth, then one could attempt to trace the temporal evolution of conditions at the CMB by studying transitional VGP clustering further back in geological time.

At a more basic level, there are other unresolved questions. For example, do reversals require an independent triggering event, either external or internal, or are they a built-in result of instabilities in the magnetohydrodynamic processes? How much can one reversal differ from another in duration and magnetic signature? In this paper we attempt to gain additional insight into all these questions by examining reversals that have occurred in supercomputer simulations of the geodynamo and comparing them with palaeomagnetic observations.

2. The simulations

Glatzmaier & Roberts (1996, 1997) have described elsewhere their physical model, including its implementation as a dynamically self-consistent computer simulation of the geodynamo. Here we give only the briefest outline. The equations describing the time-dependent thermal, compositional, velocity and magnetic fields are solved simultaneously in the three-dimensional, spherical geometry appropriate for the core. Nonlinear interactions are fully taken into account, but the short time-step required limits the spatial resolution that can be employed and still achieve usefully long simulations, even using supercomputers with parallel processors. Hence, eddy diffusion has to be introduced to represent the effects of unresolved eddies, as is done in models of the oceans and atmosphere. Thermal and compositional buoyancy produced by fractional crystallization onto the solid inner core drives the fluid motions that power the simulated dynamo in the electrically conducting fluid of the outer core. The overall strength of this convection is ultimately controlled by the rate that heat can escape from the core. This is prescribed by the heat flux through the CMB, which is held constant because it depends on the temperature gradient in the lowermost mantle, which can change only on time-scales much longer than the simulations. The lateral variation of CMB radial heat flux distribution, however, has an important influence on the structure of convection in the simulations. So far, we have investigated eight simulations with different distributions (Glatzmaier *et al*. 1999).

In this paper, we will limit our examination to two of those simulations. The first is the homogeneous case, characterized by uniform heat flux across the CMB. The total heat leaving the core is prescribed to be 7.2 TW, only 2.2 TW of which arises from the superadiabatic temperature gradient that drives convection. The second we call the tomographic case (figure 1) because it has variable heat flux over the CMB patterned after the low-order seismic velocities derived from tomographic studies of the lowermost mantle (Su *et al*. 1994): that is, more heat than average flows out of the core into faster-than-average mantle, because, presumably, it is cooler. The total heat flux through the CMB is the same as for the homogeneous case, and the peak-to-peak variation is three times the average superadiabatic heat

Downloaded from rsta.royalsocietypublishing.org

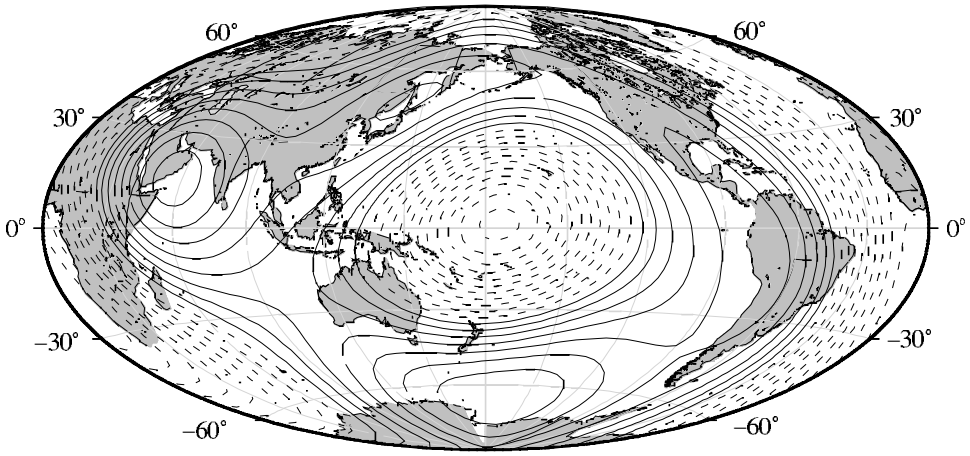

Figure 1. Pattern of heat flux at the CMB prescribed for the tomographic simulation, based on lower-mantle seismic velocity inversion of Su *et al.* (1994), as described in the text. Solid lines, values above the mean; broken lines, values below the mean. The zero of longitude is on the left.

flux (0.0446 W m^{-2}), a conservative value based on mantle convection simulations (Tackley *et al.* 1994). The numerical simulation program outputs Schmidt quasi-normalized Gauss coefficients for the scalar magnetic potential up to degree and order 21, usually at regular time-steps of *ca.* 15, 50 or 100 years. (Note that the computational time-step is much shorter: *ca.* 15 days.) From these series of Gauss coefficients, we calculated the simulated field at the Earth's surface for examination and analysis in this paper.

Both simulations have reversed twice during runs of 300 000 model years. We should emphasize from the outset that the reversals were entirely spontaneous, involving no imposed triggering of any kind. They arose from instabilities inherent in the MHD process itself, and thus argue against the need to call upon any other kind of triggering to explain geomagnetic reversals, such as the impact reversal mechanism proposed by Muller & Morris (1986).

To what extent do the fields produced by these simulations resemble observations of the geomagnetic field? As shown in figure 2, they are surprisingly Earth-like in terms of their time-averaged spatial power spectra (Lowes 1974):

$$R_n = (n+1)\sum_{m=0}^{n}[(g_n^m)^2 + (h_n^m)^2].$$

Their least-squares slopes from degree 2 to 12 are remarkably similar to those derived for the Earth from Magsat data (Langel & Estes 1982). The dipole power, R_1, dominates in all three spectra, and R_2 lies noticeably below the general trend, making a V-shaped notch that is also found in analysis of the geomagnetic field during the past 2000 years using historic and archaeomagnetic records (Hongre *et al.* 1998). However, neither the homogeneous nor the tomographic simulation reproduces the Earth's value of $g_2^0/g_1^0 = +0.04$, obtained by averaging over the last 5 Ma of palaeomagnetic records (Johnson & Constable 1995; Merrill *et al.* 1996; McElhinny *et al.* 1996). Instead, each gives approximately −0.02. In addition, both simulated spectra are distinctly lower than that for the modern field, but perhaps they should be: recent

Downloaded from rsta.royalsocietypublishing.org

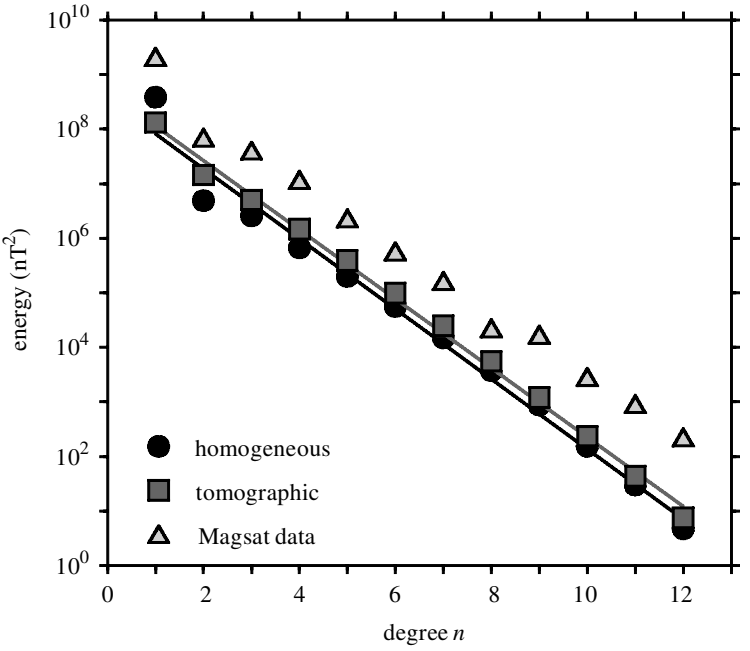

Figure 2. Magnetic field spatial power spectra at the Earth's surface. Triangles, modern Earth's field from Magsat data (Langel & Estes 1982); circles (squares), homogeneous (tomographic) simulations averaged over times when simulated field was not undergoing a reversal or an excursion.

palaeomagnetic evidence suggests that the time-averaged geomagnetic field may have been 25–50% lower than today's (Juarez *et al.* 1998; Guyodo & Valet 1999). Finally, with regard to secular variation, both simulations give VGP dispersions from equator to pole that are much flatter than the Earth's over the past 5 Ma, varying by only 1 or 2°. For the homogeneous case, the dispersion is approximately the Earth's equatorial value, and for the tomographic case the Earth's polar value.

To sum up, both simulations differ in several regards from current palaeomagnetic characterizations of the time-averaged field over the past 5 Myr. In the following sections we will show, however, that despite these differences the simulated reversals resemble real reversal records in some aspects and suggest additional insights in others.

3. The simulated reversals

(*a*) *Homogeneous case*

In this paper, we analyse and show results for a run of 315 kyr. It was preceded by 150 kyr of simulation during which the Gauss coefficients were saved only infrequently. The first reversal occurred roughly 90 kyr into the run, that is, 240 kyr after the simulation began, which is plenty of time—11 free decay times for the field in the core—for any transient behaviour stemming from the initial conditions to die away. It was followed by a second reversal *ca.* 170 kyr later. These reversals stand out in figure 3*a*, which shows the variation of dipole and non-dipole energy density averaged over the Earth's surface (R_1 and $\sum R_n$ for $n = 2$–21, respectively). The

Downloaded from rsta.royalsocietypublishing.org

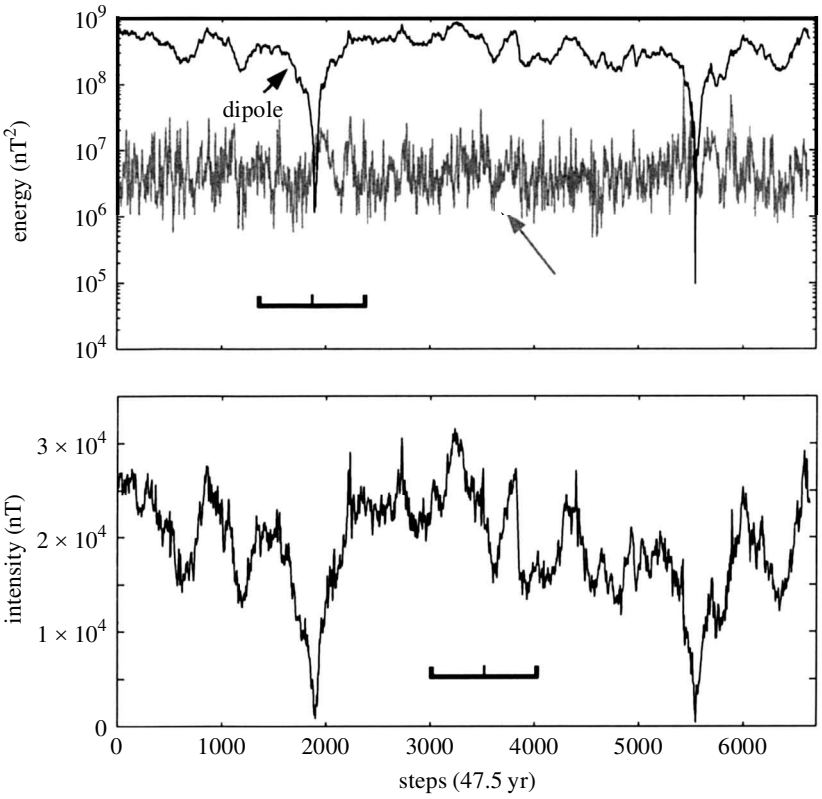

Figure 3. Homogeneous simulation. (*a*) Energy density at Earth's surface of the dipole and non-dipole fields. The field reversed at the two sharp drops of the dipole. (*b*) Dipole field intensity as observed at location 40° N, 240° E.

sharp drops in dipole energy by two to three orders of magnitude, down to or even well below the non-dipole field energy, mark the polarity transitions. Note as well the long-term decrease in dipole energy leading up to each of the reversals. This is shown more clearly in figure 3*b*, in terms of field intensity plotted on a linear scale, and will be discussed later.

The duration of the first reversal of the homogeneous simulation, as defined by the drop and recovery in dipole intensity, can be estimated in figure 3*b* and in the more detailed view provided in figure 4*a*, *b*. The axial dipole intensity transition low measures anywhere from 6 to 24 kyr, depending on whether it is defined as the time spent below 9000 or 18 000 nT, respectively. Extrapolation downward of the long-term intensity decrease before each reversal (figure 3*b*) shows that the shorter period is a more reasonable characterization of the reversal itself. The total field intensity (figure 4*b*) at this site (40° N, 240° E) preserves the basic form of the dipole intensity, while fluctuating about it, and so also yields similar estimates of duration.

The transition in directions during the reversal can also be variously defined. Figure 4*b* shows the change in local field direction at 40° N, 240° E from stable normal to stable reversed in terms of the reversal angle, i.e. the angle between the direction of the observed field and the normal polarity geocentric axial dipole field. It took just 1.6 kyr for the direction to swing 145°, but 7.7 kyr to span between fully

Downloaded from rsta.royalsocietypublishing.org

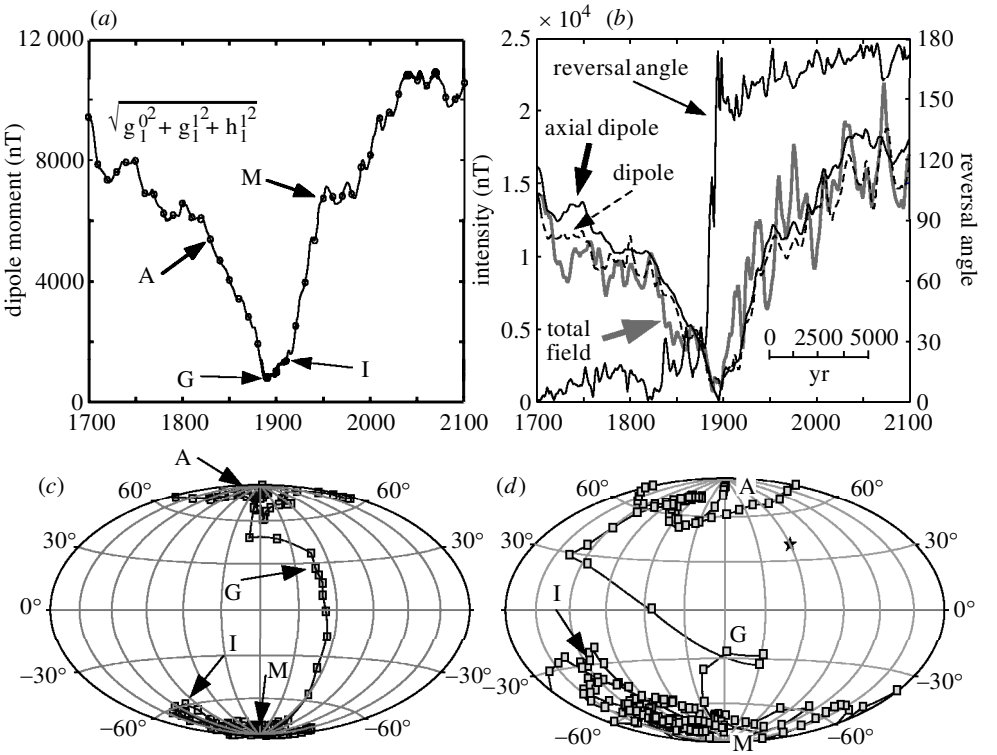

Figure 4. First reversal (normal to reversed) of the homogeneous simulation. (*a*) Dipole moment (normalized by radius cubed of the Earth) versus time-step. (*b*) Left axis, axial dipole, dipole and total field intensity; right axis, reversal angle, as observed for each time-step at location 40° N, 240° E. (*c*) True dipole path. (*d*) Virtual geomagnetic pole path, as observed at location 40° N, 240° E. Every tenth time-step (every 475 yr) between steps 1830 and 1950 corresponds to a letter A–M, as shown. The observation site is indicated by a star.

antipodal states. In contrast, the dipole field took only 0.6 kyr to swing from normal to reversed, or 1.3 kyr until it completely settled down (figure 4*c*). The path taken by the dipole as it turned over in this reversal is simple and longitudinally confined, and it continues past the South Pole along the antipodal longitude in a small excursion to a point a little beyond 60° S before returning to fully stable reversed polarity. The full field transition path, as expressed by VGPs, is, of course, more complex and longer in duration, reflecting the effect of the non-dipole field superimposed on the reduced dipole field (figure 4*d*). At different observation sites, the VGP paths for this reversal differ greatly, as shown by several examples in figure 5. Depending on where the reversal is observed and one's definition of transitional VGP latitudes, the duration of the reversal ranges from 2.0 to 6.4 kyr.

The second reversal of the homogeneous simulation is very similar to the first in regard to dipole intensity variation (figures 3*b* and 6*a*). Not counting the long-term variation, the duration of the axial dipole intensity dip that is associated with the reversal is *ca.* 6 kyr. The local intensity low and directional instability of the total field at 40° N, 240° E are also *ca.* 6 kyr in length (figure 6*b*), but much more rapid swings away from the axial dipole direction occur within this interval: more than

Downloaded from rsta.royalsocietypublishing.org

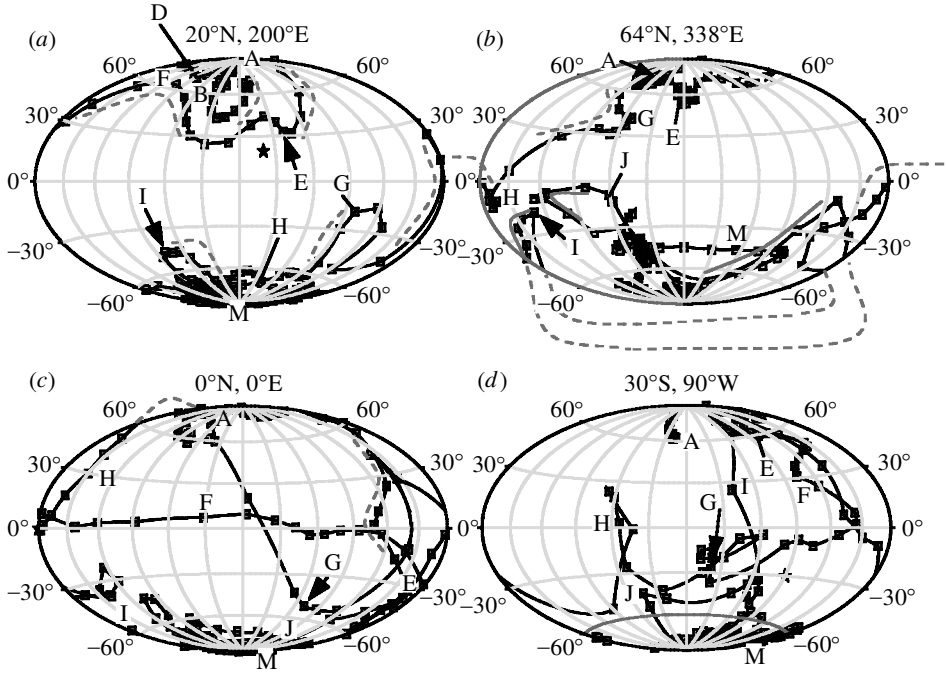

Figure 5. VGP paths for first reversal of the homogeneous simulation as observed at (*a*) 20° N, 200° E, (*b*) 64° N, 338° E, (*c*) 0° N, 0° E, and (*d*) 30° S, 90° W. Letters and star are as described in the caption of figure 4.

100° in reversal angle in 150 years at rates reaching at least 1° per year. The dipole transition path is more complex than for the first reversal, with a general trend westward and with several large swings in longitude spanning 60–120° (figure 6*c*). The rate of movement of the pole during one of these swings was unusually rapid, jumping 60° to the west and 40° northward across the Equator in just 50 years, even though the full 180° reversal from stable reversed to stable normal took 3.2 kyr. As the pole traversed from 60° S to 60° N, it made one complete revolution about the globe in longitude. As we saw for the first reversal, the VGP paths vary a great deal in geometry and duration between distant sites on the globe, but one common feature displayed by many of them is prominent westward looping (figure 6*d*). In duration, the local field reversals range from as little as 2 kyr to more than 6 kyr.

(*b*) *Tomographic case*

The tomographic simulation, like the homogeneous simulation, has also reversed twice in 300 kyr. In some other respects, however, it is rather different. Very prominent, sharp peaks in non-dipole field energy occurred every 40–50 kyr, one to two orders of magnitude above the background value (figure 7*a*). Most of them coincided with smaller peaks in dipole energy. In addition, there are almost as many order-of-magnitude or greater dips in dipole field energy, some of them precipitous. Of course, the intensity of the dipole field shows corresponding peaks and troughs (figure 7*b*).

In contrast to the homogeneous case, it would not be easy to guess where the two reversals occurred in figure 7 without prior knowledge. The first reversal happened

Downloaded from rsta.royalsocietypublishing.org

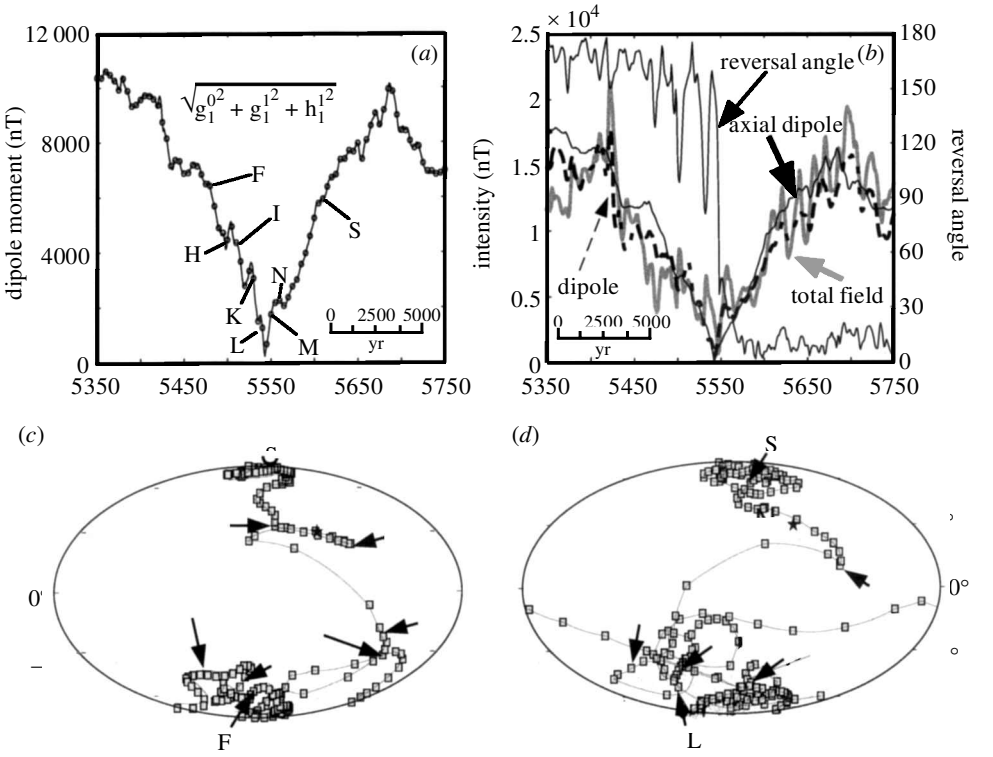

Figure 6. Second reversal (reversed to normal) of the homogeneous simulation. Every tenth time-step (every 475 yr) between steps 5480 and 5610 corresponds to a letter F–S, as shown. See caption of figure 4 for full description.

suddenly, with no warning given by a preceding long-term decrease of dipole intensity; in fact, the intensity was slowly climbing when the reversal began. Its duration, defined by the initial sharp drop and the final rapid recovery of dipole strength, is 2.5 kyr (figure 8*b*). The inversion of the dipole occurred in several stages, the swings in its orientation confined mainly to longitudes between 245 and 305° E longitude and corresponding closely in time with the falls and rises in its intensity (figure 8*c*). The pole first moved rapidly from normal to reversed polarity in 0.4 kyr as the dipole intensity dropped by 40% and then quickly recovered. During the next 0.5 kyr, the pole rebounded to 30° N as the intensity plummeted to 20% of its pre-transition value. In the 1.0 kyr third stage, the dipole grew to a relative maximum of 75% of pre-transitional as the pole reached the Equator, then dropped to a relative minimum and recovered as it passed through low into high southern latitudes. In the last stage the dipole made a second, smaller excursion to 50° S and back as the intensity climbed to a maximum 60% greater than pre-transitional and returned to around the initial value.

The non-dipole field fluctuations during this first reversal of the tomographic simulation caused especially large local variations in the transition signature. At 40° N, 240° E the reversal in direction took *ca.* 4.5 kyr, during which time the intensity went through two large peaks and never dropped significantly below the pre-transition background value (figure 8*b*). The VGP record is significantly more complex than

Downloaded from rsta.royalsocietypublishing.org

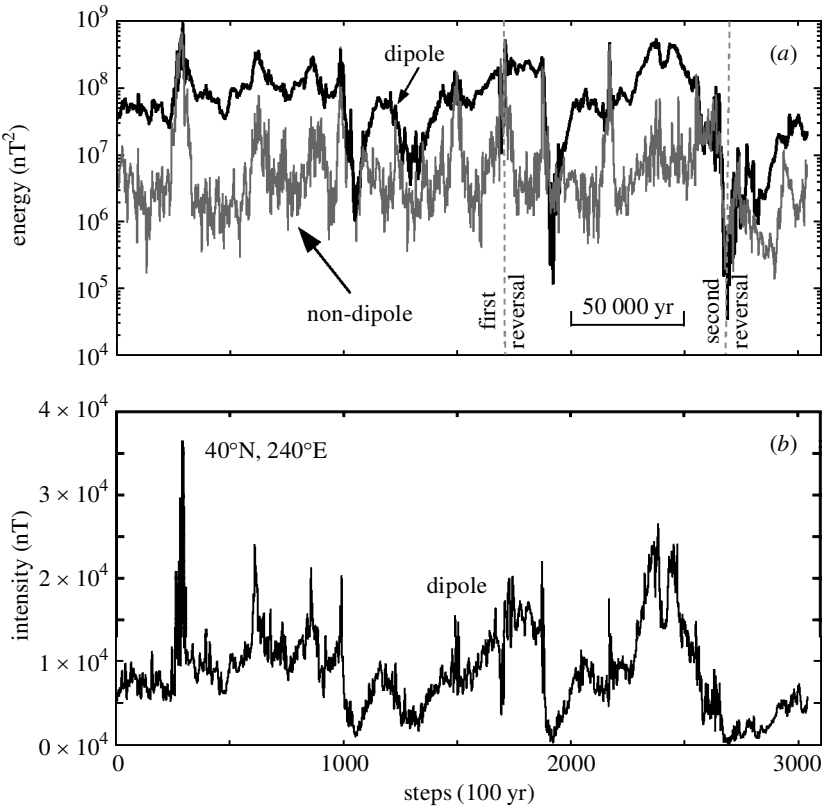

Figure 7. Tomographic simulation. (*a*) Energy density at Earth's surface of the dipole and non-dipole fields. (*b*) Dipole field intensity as observed at location 40° N, 240° E.

that for the true dipole, with more small excursions both before and after the polarity switch. Some similarities remain in the structure of the main transition, however, despite the importance of the non-dipole field. The rapid initial reversal is followed immediately by a large and then by a smaller excursion, and most of these VGPs lie in the same range of longitudes as the dipole poles. At this location reinforcement occurs between dipole and non-dipole field, as clearly shown by comparing the variation in total field intensity and the dipole moment in figure 8*a*, *b*. At many other locations, however, the transition signature looks more like high-resolution palaeomagnetic records of real reversals. For example, the record in figure 9*a* is much like the Steens Mountain reversal record (Mankinen *et al*. 1985; Prévot *et al*. 1985*a*, *b*), showing the usual pronounced low-intensity interval down to 20% of the pre-transition value, a rebound from intermediate directions back to the initial polarity, and completion of the reversal followed by oscillating high values as much as 70% above the pre-transition intensity. Figure 9*b* shows an even more typical signature at another location, with nearly equal pre- and post-transition intensities.

The second tomographic reversal is much longer and more complex than the other reversals. The magnetic field energy density, both dipole and non-dipole, dropped very low and was still recovering very slowly by the end of the run (figure 7*a*). Thus, one cannot define the duration well in terms of the intensity, but it would be more

Downloaded from rsta.royalsocietypublishing.org

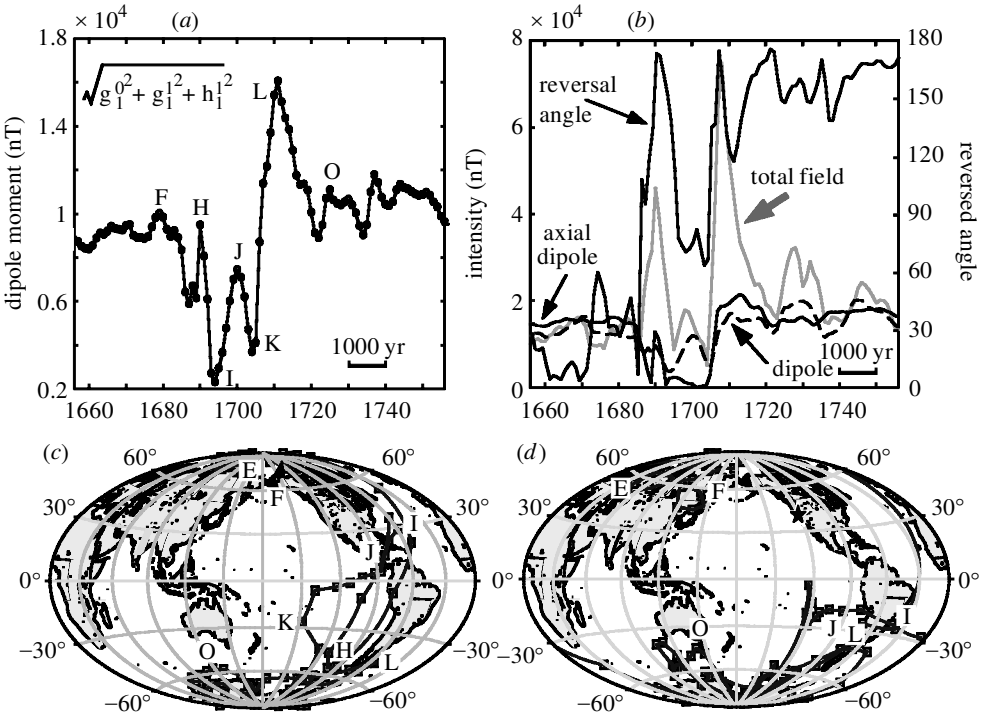

Figure 8. First reversal (normal to reversed) of the tomographic simulation. Every fifth time-step (every 500 yr) between steps 1680 and 1725 corresponds to a letter F–O, as shown. See caption of figure 4 for full description.

than 50 kyr at 40° N, 240° E (figure 7*b*). In terms of reversal angle, including all the significant excursions except the last large excursion in figure 10*b*, the transition took 22 kyr. The reversal began with a series of six increasingly large excursions from reversed polarity as the intensity dropped from 10^4 to less than 10^3 nT over a period of 12 kyr. In the middle 3 kyr of the transition, while the intensity was below 400 nT, the field swung seven times between reversed and normal polarity. The reversal ended with five more excursions from normal polarity in 7 kyr as the field intensity slowly increased. In addition, at the beginning and end of the first part of the transition, the dipole moment underwent several large, rapid oscillations in strength (figure 10*a*). Both the dipole and the VGP paths are naturally complex as well (figure 10*c*, *d*). The dipole path displays much east–west movement and few instances where the pole crosses the Equator. The effect of the non-dipole field is to increase the component of north–south movement and, thus, to double or triple the number of equatorial crossings of the VGP.

A palaeomagnetist confronted with a rock record like this would, most likely, disregard it, ascribing the multiple swings in direction to variable remagnetization of primary reversed remanence by a later normal field. If not, the reviewers probably would, so it would be unlikely to get published. Yet we have no reason to be sure that the Earth's field could not undergo such a complex reversal. In fact, there is one published article of a reversal record that estimates a duration as long as 28 kyr for the Lower Olduvai transition (Herrero-Bervera *et al*. 1987). It is interesting that this appears to

Downloaded from rsta.royalsocietypublishing.org

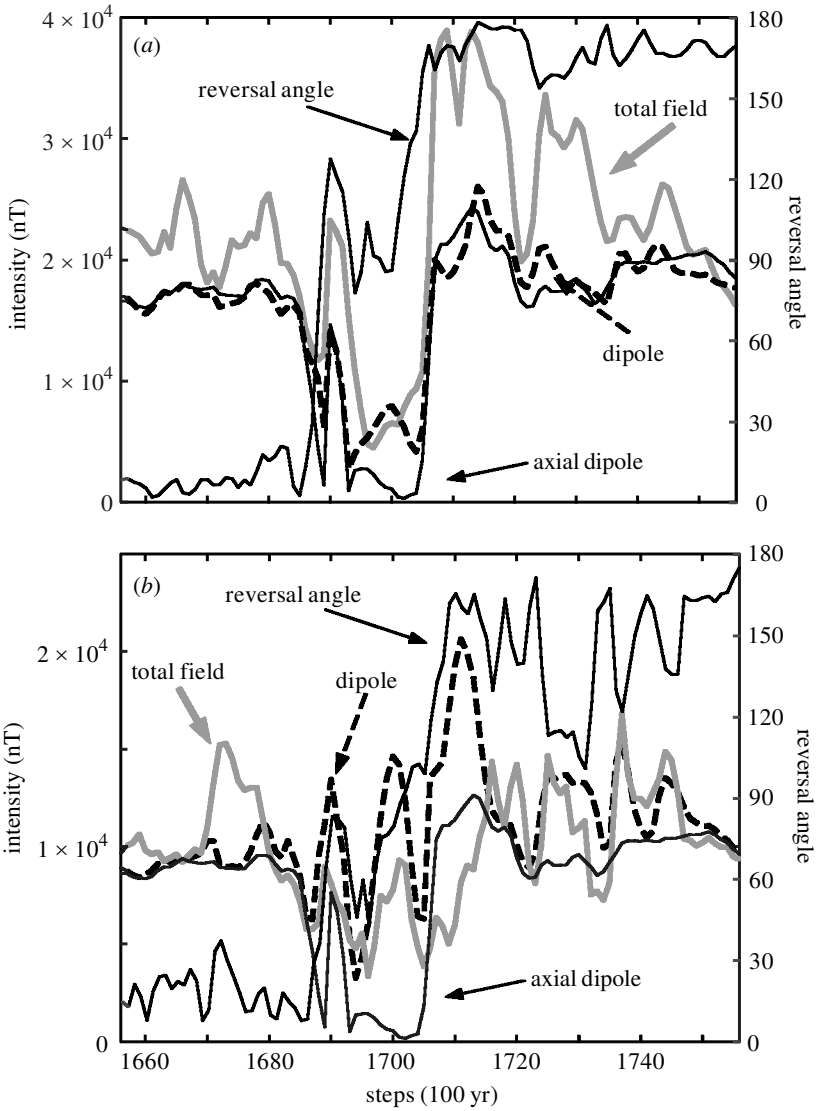

Figure 9. First reversal of the tomographic simulation observed at 64° N, 338° E (*a*) and 0° N, 75° E (*b*). Left axis, axial dipole, dipole and total field intensity; right axis, reversal angle.

be the only published reference for this transition, although there are six or seven for the Upper Olduvai. Could it be that other studies of this transition have been conducted but not published because the record seemed to be 'unrealistically' complex?

4. Further characterization and discussion

(*a*) *Initiation of reversals*

The abruptness of geomagnetic reversals and their irregular spacing in time have long encouraged proposals that they are triggered by events external to the core, such as

Downloaded from rsta.royalsocietypublishing.org

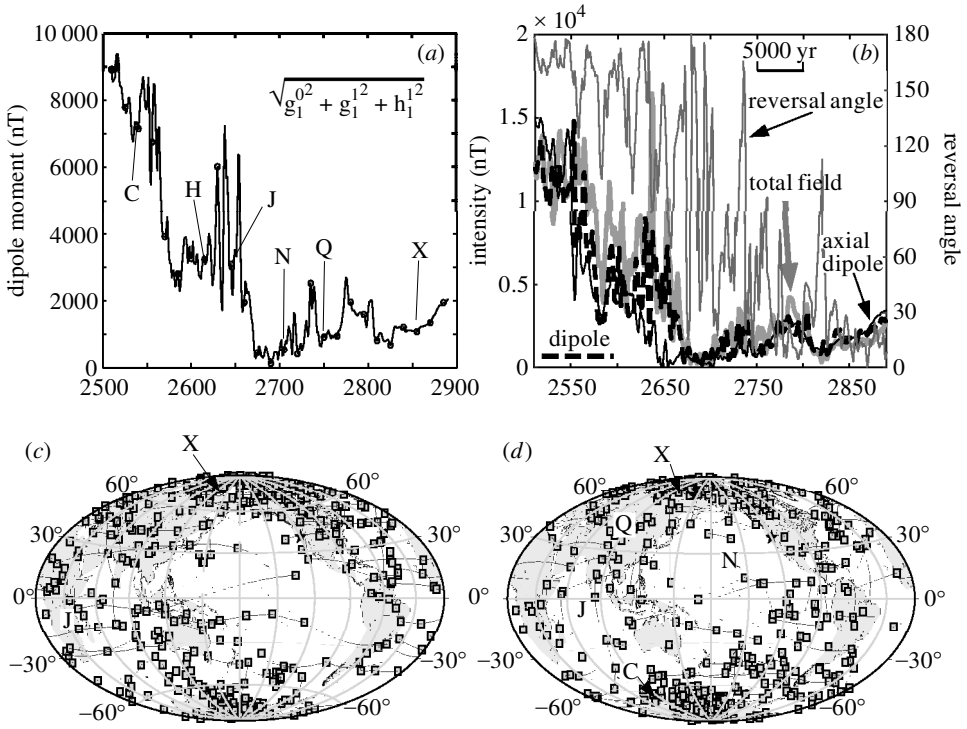

Figure 10. Second reversal (reversed to normal) of the tomographic simulation. Every 15th time-step (every 1500 yr) between steps 2540 and 2855 corresponds to a letter C–X, as shown. See caption of figure 4 for full description.

earthquakes (Heirtzler 1970) or meteorite impacts (Glass & Heezen 1967; Muller & Morris 1986). These suggestions have been contested on observational and theoretical grounds (Merrill & McFadden 1990; Jacobs 1994); they are not supported by the present simulations, in which the reversals are entirely spontaneous. No triggering event of any kind is imposed; the reversals arise from the evolving solution of the governing equations alone. Thus, it is unnecessary to call upon external triggering for the Earth's reversals, although one cannot rule out the possibility that it may have occurred on occasion.

On the other hand, McFadden & Merrill (1986) proposed an internal source for reversals. They concluded from their statistical analysis of polarity intervals that triggering must be effectively independent of the main process driving the geodynamo, suggesting that the compositional convection due to crystallization of the inner core mainly produces the field, and thermal convection due to cooling at the CMB produces cold blobs of descending fluid that are sometimes large enough to disorganize the pattern of flow and trigger convection. In the simulations, however, both compositional and thermal buoyancy are important and produce magnetic effects that are inextricably intertwined. Significant latent heat is released at the same places as compositional sources of buoyancy, and both are advected and diffused upward in the same way. Thus, they cannot be assigned exclusive roles as field generator and reversal trigger. Moreover, we have not seen unusually large descending blobs that

Downloaded from rsta.royalsocietypublishing.org

PHILOSOPHICAL TRANSACTIONS OF THE ROYAL SOCIETY A MATHEMATICAL, PHYSICAL & ENGINEERING SCIENCES

stand out as probable triggers. The simulations seem to be chaotic enough that they do not need a trigger, internal or external. It is true, however, that all of the simulated reversals that we have examined in detail for these cases began in the outer part of the outer core and propagated inward (Glatzmaier *et al.* 1999), as predicted by McFadden & Merrill (1986).

Despite the difficulty in identifying specific triggers, it is worthwhile to examine the characteristics of the simulated magnetic field before the reversals occurred. In 1968, Cox proposed that when the axial dipole field decreases to a low enough value relative to the non-dipole field a random fluctuation of the latter could change the sign of the former and seed a reversal (Cox 1968). This idea could not be quantified rigorously because palaeomagnetic data are never complete enough to unambiguously separate them into dipole and non-dipole parts. Nonetheless, Cox (1968) showed that such models are not only consistent with low field intensity during reversals, but can also explain the Poisson-like distribution of geomagnetic polarity intervals. With the luxury of simulated data, which are global and closely spaced in time, we can examine this idea using Lowes's energy density parameter, R_n, for the dipole and non-dipole fields (figures 3*a* and 7*a*).

The homogeneous case is dipole dominated (figure 3*a*), even more so than the Earth's present field (figure 2). Except around times when it was reversing, the dipole energy density was typically between 2×10^8 and 6×10^8 nT^2 and the non-dipole energy density between 1×10^6 and 2×10^7 nT^2. For both reversals there seems to be a threshold value *ca.* 10^8 nT^2 for the energy density, below which the dipole field collapsed and switched polarity. In both instances, the general trend of the non-dipole energy leading up to the collapse was upward. For the second reversal, but not for the first, an order-of-magnitude larger than usual upward spike in non-dipole energy began just before the dipole energy dropped quickly from 2×10^8 to 1×10^8 nT^2, and shortly thereafter the dipole intensity plummeted and the field reversed (figure 6). Although necessarily based on just two occurrences, we suggest the following interpretation. In the homogeneous simulation, reversals can be readily triggered by typical non-dipole field fluctuations when the dipole energy is 1×10^8 nT^2 and the general trend of the non-dipole energy is rising. An exceptionally large non-dipole fluctuation can raise the dipole energy stability threshold to 2×10^8 nT^2. Why both attempts at reversal were successful, i.e. there were no significant excursions, is an interesting question. It could be a long-term characteristic of this case, but more probably it is coincidence. Answering this question will require extending the simulation.

As mentioned previously, the variation of dipole intensity shown in figure 3*b* for the homogeneous simulation is reminiscent of the relative palaeointensity record derived by Valet & Meynadier (1993) from marine sedimentary cores. For about half of that record, the intensity displays a sawtooth behaviour, oscillating widely with a period of *ca.* 30 kyr about a long-term decreasing trend until it collapses at a reversal boundary and builds back up with opposite polarity. Extrapolating the decreasing trend of the relative minima to the intensity drop at the reversal yields a threshold for onset of reversal 30–40% of the long-term average. The homogeneous simulation displays large-intensity oscillations of similar period about a long-term trend that decreases at a similar relative rate (figure 3*b*), with a reversal threshold estimated in the same way at 50% of the long-term average. After both reversals, the intensity regenerated to a peak value 50% higher than before.

Downloaded from rsta.royalsocietypublishing.org

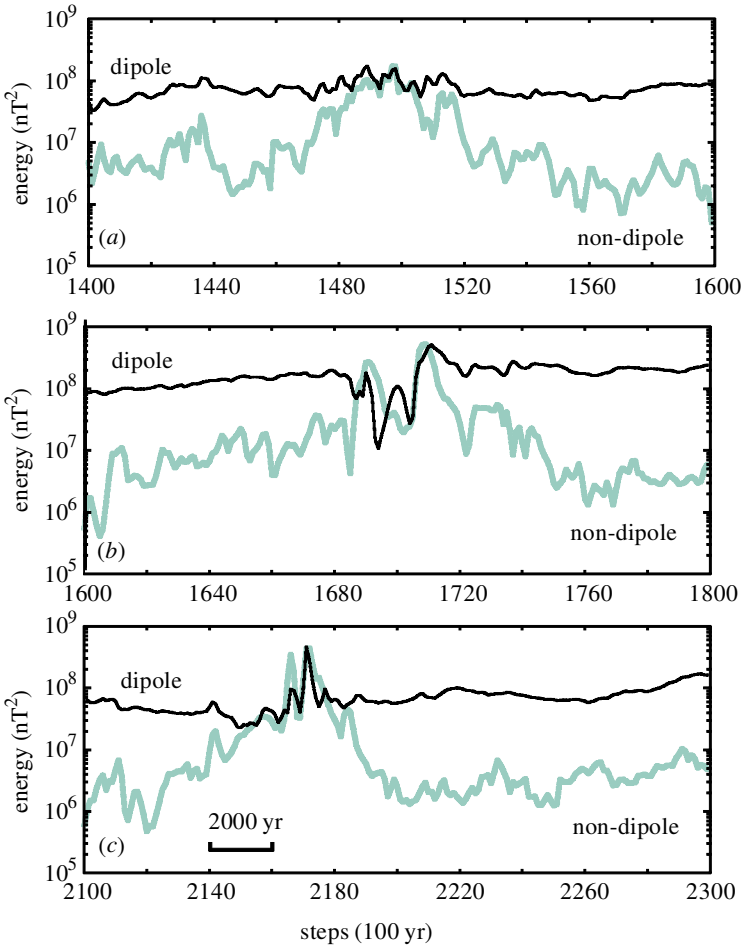

Figure 11. Energy density at the Earth's surface of the dipole and non-dipole fields for the tomographic simulation. (*a*) Excursion 20 kyr before the first reversal; (*b*) first reversal; (*c*) excursion 48 kyr after the first reversal. See figure 7*a* for entire record. Note that for the successful reversal in (*b*) the initial large increase of the non-dipole energy around step 1685 occurred as the dipole energy was falling, whereas with the excursions the case was the opposite.

The tomographic simulation is much less dipole dominated than the homogeneous simulation, and considerably less so than the Earth (figure 2). It is also less stable. Both the dipole and non-dipole energy density records exhibit a number of large, rapid fluctuations, both up and down (figure 7*a*). There are three events where the dipole energy dropped by at least two orders of magnitude, and three others where the drop was about one order of magnitude. One large and one small drop were accompanied by a global reversal of polarity. As in the homogeneous case, for both reversals the trend of the time-averaged non-dipole field was upward during the time leading to the dipole collapse. Otherwise, though, these reversals are quite different from those of the homogeneous simulation.

The first tomographic reversal began when the long-term dipole intensity was *stronger* than average and increasing. It seems to have been initiated by the sudden

Downloaded from rsta.royalsocietypublishing.org

PHILOSOPHICAL TRANSACTIONS OF THE ROYAL SOCIETY A MATHEMATICAL, PHYSICAL & ENGINEERING SCIENCES

appearance of a pair of exceptionally large non-dipole field features (figure 13*b*), which we will discuss further later. An upward kick in the non-dipole field strength coincided with an initial dip in dipole energy that ushered in a further drop and rapid reversal (figure 11*b*). The dipole intensity recovered 2.5 kyr later and continued its long-term trend as though it had not been interrupted. Two other comparable non-dipole spikes, around steps 1500 and 2200, only produced short-lived excursions. In both these cases the largest non-dipole field energy peaks were in phase with dipole energy peaks (figure 11*a*, *c*), whereas reversal seems to be favoured when they are initially significantly out of phase.

The second tomographic reversal occurred during the third large collapse of the dipole field. As described earlier, the time of directional instability is long and recovery of intensity is slow. Each of the three large dipole collapses terminated an *upward* trend in the long-term energy, as though there were an upper threshold *ca.* 3×10^8 nT^2 for the tomographic case, *above* which the field is unstable. This is just the opposite of what happened in the homogeneous simulation.

(*b*) *Space-time variation*

It is not easy to portray the complex character of the simulated reversals, but it is important to do so because we have every reason to believe that real reversals are at least as complex. As has been noted by many workers, the magnetic signature of a reversal will vary with location because of the spatial and temporal variability of the non-dipole field (Clement & Kent 1984). Describing the temporal variation at even a single site can be complicated because of the rebounds and excursions that typically occur and what is really needed to describe the entire phenomenon is the space-time variation of the polarity transition around the globe.

In figure 12, we attempt to illustrate the nature of the space-time variation for the two homogeneous and the first tomographic reversals. We use the colour spectrum to indicate the progression of the polarity transition in terms of VGP latitude, which is still only part of the story because it neglects the simultaneous variation of VGP longitude and field intensity. Each diagram shows the space-time variation of VGP latitude at all site longitudes around a particular circle of latitude. In figure 12, we only show the variation at the Equator and at 65° N and 65° S, but we have examined the space-time behaviour at other intermediate and higher latitudes. If the field were purely dipolar, all sites would record the same VGP latitude at the same time and the boundaries on the diagrams would be vertical lines at exactly the same time-step.

The first reversal of the homogeneous simulation shows considerable temporal variation over the globe. The best marker to track is where the VGP crosses zero, as shown by the dashed line in figure 12, because this is the midpoint of the transition zone and is the same for both VGPs and directions. The VGP first crosses zero in the equatorial region from 330° eastward to 75° E longitude near time-step 220, but oscillates in polarity several times before finally staying reversed around time-step 270–275. Figure 5*c* shows the full VGP path for a site in this region, which involves much longitudinal motion not shown in figure 12, in addition to the several equatorial crossings. Most of the equatorial sites, however, reverse around time-step 250 and stay reversed. Tracking the reversal poleward, the reversal boundary becomes simpler and occurs later, at time-step 265 in the north and 285 to 290 in the south. The maximum time difference for the final VGP crossing is almost 2000 years between

Downloaded from rsta.royalsocietypublishing.org

PHILOSOPHICAL TRANSACTIONS OF THE ROYAL SOCIETY A MATHEMATICAL, PHYSICAL & ENGINEERING SCIENCES

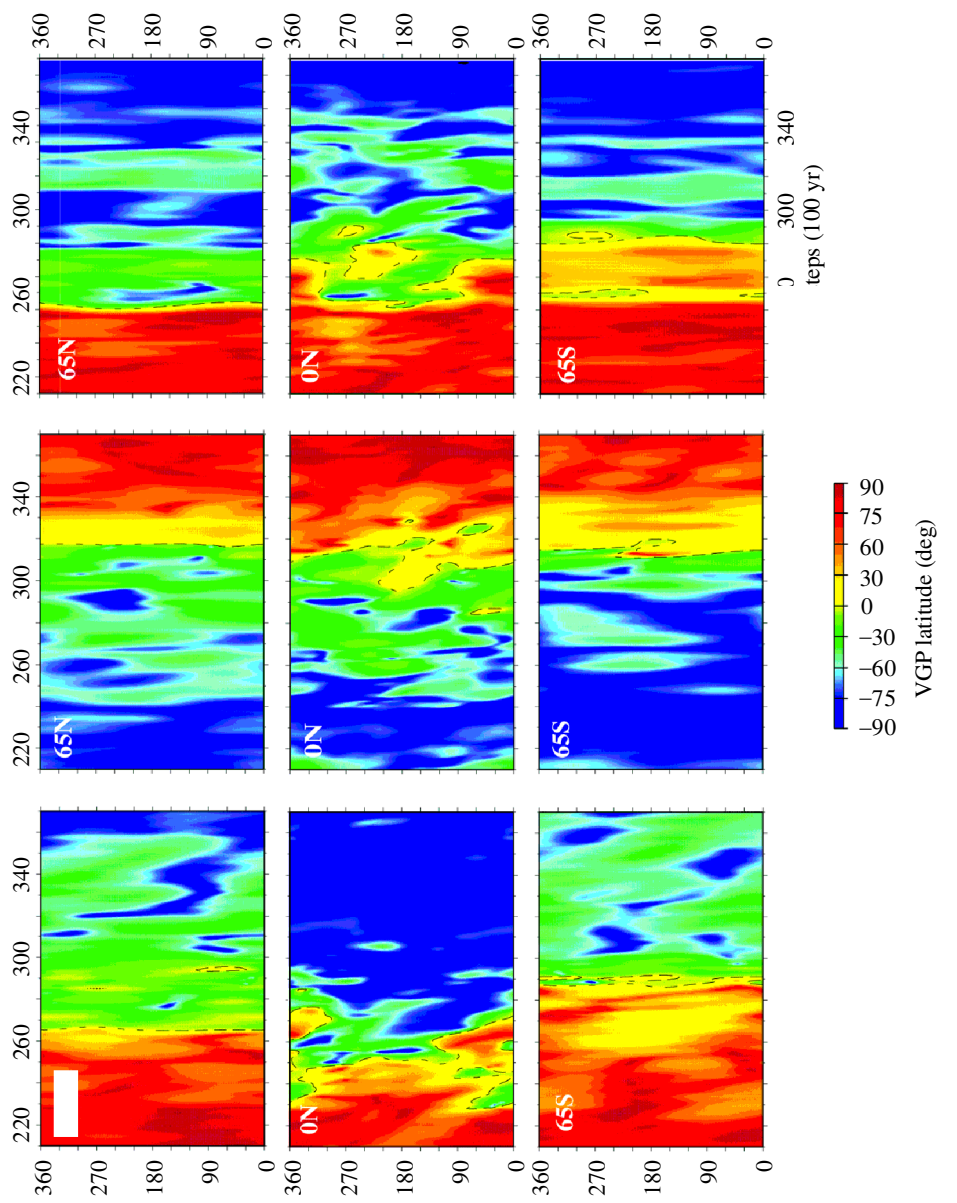

Figure 12. Space-time variation of VGP latitude (colours) for homogeneous first reversal (left column), homogeneous second reversal (centre column) and tomographic first reversal (right column) at all sites around circles of longitude at latitudes of 65° N (top row), 0° N (centre row) and 65° S (bottom row). The broken line indicates a VGP latitude of 0°.

the Equator and the South Pole. Roughly speaking, this reversal can be characterized as starting in a region near the Equator and propagating both longitudinally and poleward, something like the idealized flooding models proposed 20 years ago by Hoffman (1979).

Downloaded from rsta.royalsocietypublishing.org

PHILOSOPHICAL TRANSACTIONS OF THE ROYAL SOCIETY A MATHEMATICAL, PHYSICAL & ENGINEERING SCIENCES

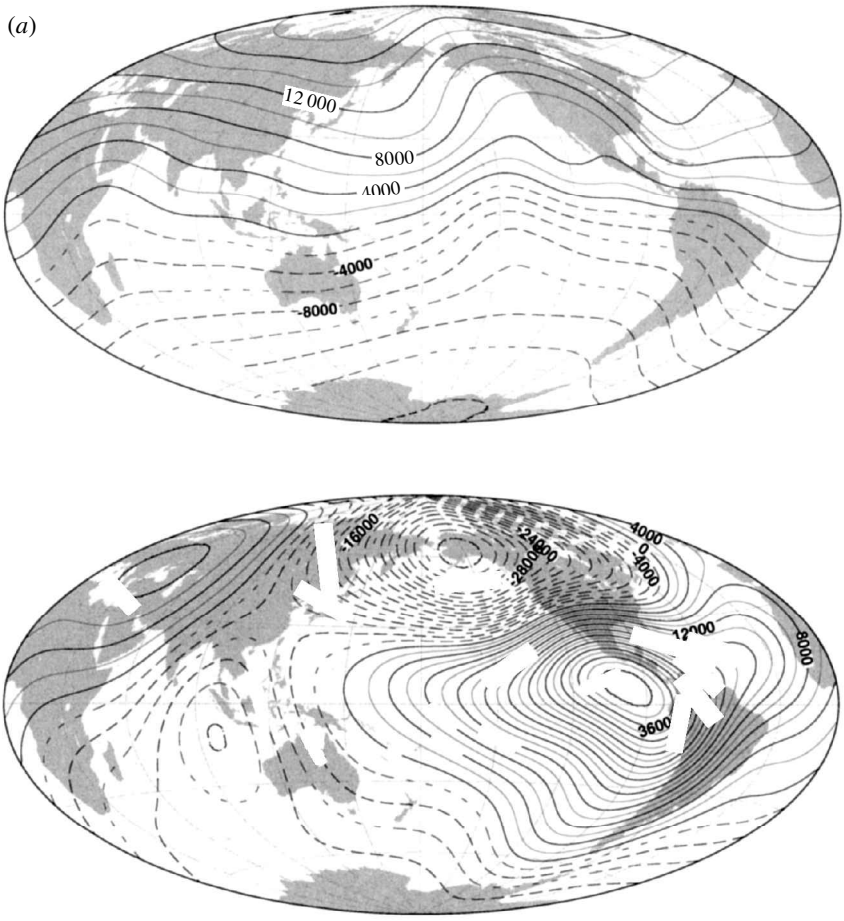

Figure 13. Vertical field for tomographic simulation at time-step just before the first reversal (*a*) and 400 years later (*b*). These steps correspond to the fifth and first points, respectively, before point H on figure 8*a*. Solid contours indicate downward field, broken contours upward, and contour interval is 2000 nT. The appearance of the flux patches in (*b*) marked the reversal of polarity at high northern latitudes and (temporarily) at the Equator near 180° E (see figure 12).

The second homogeneous reversal is much less time transgressive. The maximum time difference for the final VGP crossing for sites around the globe is 800 years, and for the great majority it is less than 500 years (figure 12). The reversal signature is more complicated at low latitudes than at high latitudes and, generally, takes longer to complete in the Northern Hemisphere than in the Southern Hemisphere.

The first reversal of the tomographic simulation is very interesting. Like the first homogeneous reversal, it is markedly time transgressive. At high northern latitudes, the VGP only traverses the Equator once, around time-step 100 of figure 12. At high southern latitudes, there is an excursion *ca.* 400 years later, but the field does not finally reverse until 2000 years after it does in the north. At the Equator, the picture is more complicated, but has intermediate characteristics of both the north and the south (figure 12). Examination of vertical field maps around the time-step when the

Downloaded from rsta.royalsocietypublishing.org

PHILOSOPHICAL TRANSACTIONS OF THE ROYAL SOCIETY A MATHEMATICAL, PHYSICAL & ENGINEERING SCIENCES

field first reversed shows what happened (figure 13). Within only 100 years (one time-step), a pair of large non-dipole field foci of opposite sign suddenly appeared and grew in place to 40 000 and −32 000 nT, doubling and quadrupling, respectively, within just 300 years. These reversed the field at high northern latitudes and, temporarily, at the Equator between longitudes 90 and 300° E.

The second tomographic reversal record is too long and complex to illustrate here in a single space-time diagram. To briefly summarize, the onset of reversal was extraordinarily time transgressive. If for simplicity we define it as the first time the VGP crosses zero latitude, it occurred first in the Southern Hemisphere and did not reach high northern latitudes until 11 kyr later. Yet the last VGP crossing occurred 3 kyr earlier at the North Pole than at the South Pole. Thus, by this definition the reversal took 22 kyr in the south and only 8 kyr in the north.

(*c*) *Transition morphology*

The geometry of the transition field during reversal of the geomagnetic field is a question that has vexed palaeomagnetists and theoreticians for a long time. Various idealized schemes for polarity reversal have been entertained, one of the simplest being that the dipole simply turns over, so that the field at the midpoint of the transition is that of an equatorial dipole superimposed on the non-dipole field. An even simpler model is that the axial dipole decays to zero and regenerates with opposite sign, leaving the non-dipole field as the transition field. These ideas can be mixed and the strength and structure of the non-dipole field can be adjusted to achieve an infinite variety of transition field models. Because the duration of reversals is generally much less than the calculated free decay time of the dipole field in the core, it is logical to ascribe them to active processes and to assume that some or all of the dipole field energy is transferred into the non-dipole field. Several models for doing this have been proposed, all phenomenological rather than physical. Flooding models postulate that reversal of an assumed uniform dipole field source region nucleates locally in the core and spreads regularly throughout the region (Hoffman 1977, 1979; Williams & Fuller 1981). If it starts at one pole, at the middle of the transition when the reversal region equals the still unaffected region in size, the dipole field will be zero, and the opposing hemispheres would give rise to a dominantly axial quadrupole transition field. If the reversal nucleates at points all around the Equator, the transition field would be an axial octupole, and if it nucleates at a general point, the transition field will include both zonal and non-zonal terms. Other models specifying simple ratios of low-order Gauss coefficients that grow at the expense of the dipole have been concocted in an attempt to fit aspects of particular reversal records (Fuller *et al*. 1979; Herrero-Bervera & Theyer 1986; Clement & Kent 1991; Clement 1991). A problem with this approach is that it is usually not possible to independently correlate horizons between records of the same reversal at different sites. Thus, no one has yet been able to invert transition records for the Gauss coefficients.

Even though we know that the simulations do not accurately represent the real Earth, examining the low degree and order Gauss coefficients of the simulated reversals can help us by suggesting how simple a description of transition fields it may be useful to seek. We have conducted a detailed examination of the Gauss coefficients through the reversals, but, in this paper, we will only summarize relevant

Downloaded from rsta.royalsocietypublishing.org

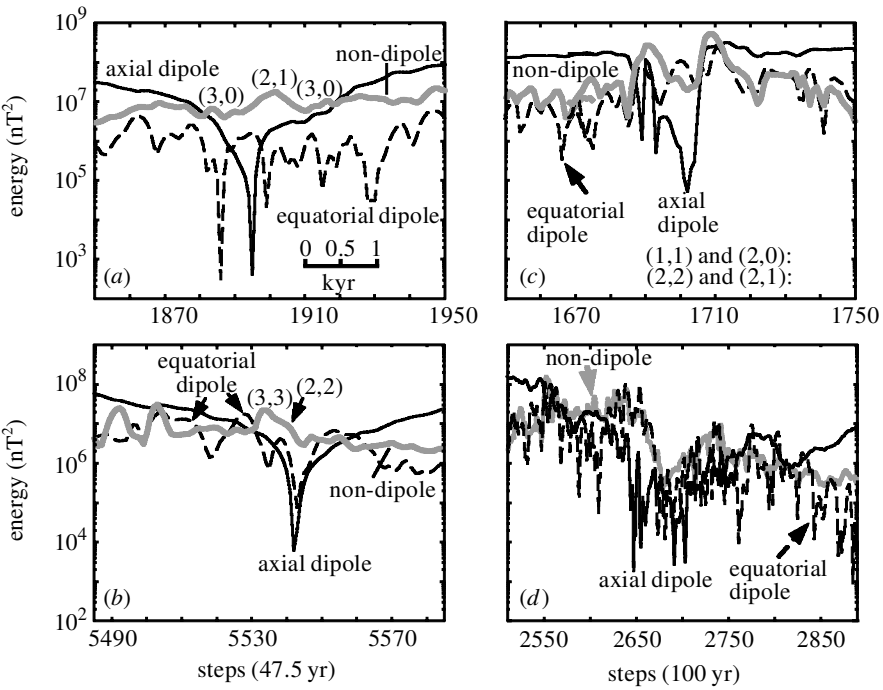

Figure 14. Detailed time evolution of the axial dipole, equatorial dipole and non-dipole energy for (*a*) homogeneous case first reversal; (*b*) homogeneous case second reversal; (*c*) tomographic case first reversal; (*d*) tomographic case second reversal. (n, m) signifies the harmonics (Gauss coefficients) that are dominant during the time-interval when the non-dipole energy is greater than both the axial and equatorial dipole energy.

results. Figure 14 shows the variation of axial dipole, equatorial dipole, and non-dipole field energy densities through the transition intervals of the four reversals. The most important part from the standpoint of transitional directions is where the axial dipole energy is less than or equal to either the equatorial or non-dipole energies.

During the first homogeneous reversal, the non-dipole energy is always larger than the equatorial dipole energy, very significantly so in the last three-quarters of the transition. (We note in passing that the equatorial dipole energy displays large, fairly regular oscillations that also show up as a large peak at a period of 600 years in spectral analyses of the entire 315 kyr homogeneous simulation.) Examination of the Gauss coefficients shows that the central peak in the non-dipole energy is mainly due to g_2^1 and h_2^1, which we will call the (2,1) coefficients, whereas the parts of the record before and after the peak are dominated by (3,0), i.e. g_3^0. These coefficients belong to the group of coefficients (n, m) with $n+m$ odd, which is called E^{A}, because they all correspond to fields that are antisymmetric about the Equator. Figure 15*a* shows the map of vertical magnetic field at the Earth's surface for the time-step when the axial dipole is closest to zero. Indeed, the field at this midpoint of the transition is mainly antisymmetric. Furthermore, as discussed above, this is the reversal that appeared to spread outward from the Equator with time in figure 12*a*, which is

Downloaded from rsta.royalsocietypublishing.org

PHILOSOPHICAL TRANSACTIONS OF THE ROYAL SOCIETY A MATHEMATICAL, PHYSICAL & ENGINEERING SCIENCES

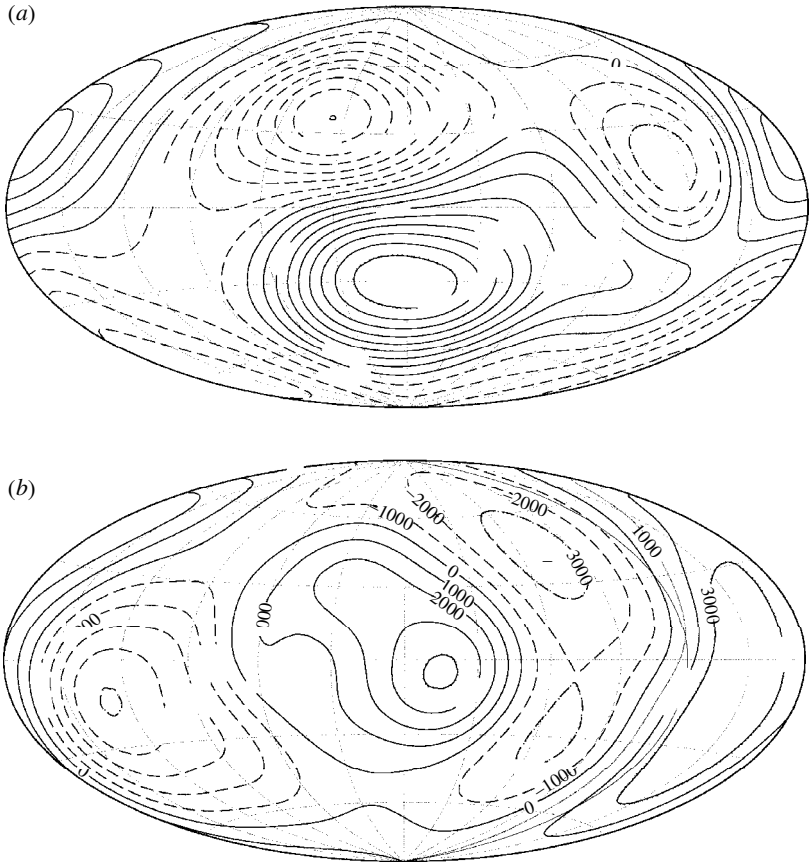

Figure 15. Vertical field for the homogeneous simulation for (*a*) the first reversal and (*b*) the second reversal at the midpoint of the transition (when the axial dipole passes through zero). Solid contours indicate downward field, broken contours upward, and contour interval is 1000 nT. Note that the field is dominantly antisymmetric about the Equator in (*a*) and symmetric in (*b*), corresponding to the odd and even values of $n+m$ for the dominant harmonics in parts (*a*) and (*b*) of figure 14, respectively.

reminiscent of one of Hoffman's (1979) flooding models. In fact, these coefficients are just the ones that Hoffman showed are largest for this particular flooding geometry.

Both the equatorial dipole (1,1) and the non-dipole field contribute significantly to the energy density for the second homogeneous reversal (figure 14*b*). The non-dipole contribution turns out to come mainly from Gauss coefficients (3,3), and to a lesser extent, but at the centre of the transition, (2,2). These coefficients represent fields that are symmetric about the Equator (E^{S}) because $n + m$ is even. They are also sectorial harmonics ($n = m$), which divide the globe into longitudinal sectors. Note that the vertical field map for the time-step at the centre of the transition is fairly symmetric about the Equator and is divided by nodal lines into four approximately longitudinal sectors (figure 15*b*). However, the temporal variation of these energy terms through the transition is large (up to an order of magnitude) and not simple.

The first reversal of the tomographic simulation is more complex than either of the

Downloaded from rsta.royalsocietypublishing.org

PHILOSOPHICAL TRANSACTIONS OF THE ROYAL SOCIETY A MATHEMATICAL, PHYSICAL & ENGINEERING SCIENCES

reversals of the homogeneous simulation. The non-dipole field energy is very high at the beginning and end of the reversal: higher than the pre- and post-transition axial dipole energy. There is a prominent rebound after a quick reversal (figure 8), so the axial dipole energy has three sharp minima (figure 14*c*). The equatorial dipole (1,1) is dominant at the last minimum, but (2,2) and (2,1) are most prominent at the second and (1,1) and (2,0) are equally prominent at the first. The vertical field map at the first minimum illustrates the large contributions of (1,1) and (2,0) (figure 13*b*). Thus, during part of the transition the field was a mixture of E^{A} and E^{S}, whereas during the rest the field was dominantly E^{S}. These changes in dominant harmonic during the transition took only a few hundred years, and the peak-to-peak energy changes in them are again about a factor of ten.

The energy density graph (figure 14*d*) of the second tomographic reversal is so complex that it defies accurate verbal description, and to show the variation of all the contributing harmonics would take many figures. Even, symmetric harmonics (1,1), (2,2) and (2,0) comprise about two-thirds of the energy averaged through this exceptionally long transition interval. Odd, antisymmetric harmonics (2,1) and (3,0) contribute the remaining one-third of the energy. The dominance of E^{S} and E^{A} fields alternates many times during the transition.

Merrill & McFadden (1990) and McFadden *et al*. (1991) found that when the angular dispersion S of VGPs of the geomagnetic field is decomposed into the parts arising from symmetric and antisymmetric harmonics, S^{S} decreases from its present value to a minimum and S^{A} increases to a maximum in the Cretaceous Normal Superchron, an interval of 35 million years when the field did not reverse at all. The variation in S^{S} correlates remarkably with the well-known variation in reversal rate during the last 160 million years (Merrill *et al*. 1996). Thus, one might suppose that the geodynamo is more likely to reverse polarity when the symmetric field is stronger and the antisymmetric field weaker, and, furthermore, that the transition field during a reversal might be dominantly symmetric. The second homogeneous and first tomographic reversals are consistent with this hypothesis. The second tomographic reversal is mixed, but broadly consistent: the symmetric contribution to the transitional field energy is about twice that of the antisymmetric components (not counting the axial dipole). The first homogeneous reversal, however, is inconsistent with the hypothesis, the antisymmetric terms (3,0) and (2,1) dominating the transition interval.

Returning to the simpler question of dipolar or non-dipolar transition fields, the four simulated reversals are all different. For the first homogeneous reversal the transition field is strongly non-dipolar throughout. For the second, the equatorial dipole field outweighs the non-dipole field at the very beginning, but the middle is dominated by the non-dipole field. The equatorial dipole dominates the middle of the first tomographic reversal, but a mixture of various quadrupolar fields are larger at the beginning and end. Finally, of the many Gauss coefficients contributing significantly to the second tomographic reversal, the equatorial dipole contributes *ca.* 30% of the non-axial-dipole energy over the long transition interval.

(*d*) *Geographical confinement of VGPs*

Debate in the palaeomagnetic community continues unabated over whether the preference shown by VGPs for longitudinal bands centred on the Americas and East Asia (Clement 1991; Laj *et al*. 1991; Tric *et al*. 1991) in many polarity transition

Downloaded from rsta.royalsocietypublishing.org

PHILOSOPHICAL TRANSACTIONS OF THE ROYAL SOCIETY A MATHEMATICAL, PHYSICAL & ENGINEERING SCIENCES

records is fact or artefact. Simple models show that the dominance of a single suitably placed flux patch could produce preferred bands for reversal paths (Gubbins & Coe 1993), but the significance of the reported banding itself has been severely questioned (Valet *et al*. 1992; Quidelleur & Valet 1994). A compilation of transitional VGPs from 0–16 Ma lava flows failed to show any preferred bands (Prévot & Camps 1993), and several explanations for banding caused by poor magnetic recording in sediments have been suggested (Rochette 1990; Langereis *et al*. 1992; Quidelleur *et al*. 1995). Nonetheless, a selection of detailed lava flow records shows clusters of VGPs in South Atlantic and Australian patches that lie on the preferred bands (Hoffman 1992, 1996). Moreover, a compilation of polarity reversals and excursions recorded by lava flows, shallow intrusive rocks, and rapidly deposited lake sediments by Glen *et al*. (1994, 1999) suggests that the transitional virtual geomagnetic poles of the geomagnetic field seen from western North America during the past 16 Myr do show a preference for two bands. These bands, however, are shifted some 30–60° east of the originally proposed bands, suggesting that their position may depend on the location of the recording site, and, thus, have a significant non-dipole field content. Most recently, in a new analysis of 0–20 Ma lava flow records, in which the data were normalized according to the number of intermediate directions, Love (1998) found a statistical bias of transitional VGPs for the longitudinal bands, which he attributed to non-zonal structure of the non-dipole field.

The question of whether preferred bands or patches do exist is important because it bears directly on lateral variations of conditions in the lowermost mantle, their influence on the geodynamo, and their implications for mantle and core dynamics (Gubbins 1994; Lay *et al*. 1998). The seismic tomography of the mantle (Su *et al*. 1994) and computer simulations of mantle convection (Tackley *et al*. 1994) suggest that the temperature in layer D^{ω} just above the CMB can vary by hundreds of degrees over lateral distances of the order of 1000 km. Lateral temperature variations at the CMB, however, are very small (*ca.* 0.001 K), because the much smaller viscosity in the fluid core makes convection much more efficient. Consequently, large variations in the radial temperature gradient must exist just above the CMB, and, therefore, also large variations in heat flux from the core to the mantle. That such variations would affect convection in the core and the operation of the geodynamo has long been noted (Cox & Doell 1964; Hide 1970). The long-term variation in reversal rate from zero in the Cretaceous Normal Superchron 100 million years ago to four or five per million years now is generally accepted to be the result of slowly changing conditions in the lower mantle (Merrill & McFadden 1990). Independent support for this interpretation is provided by these and other simulations, which show that some patterns of CMB heat flux have much higher reversal rates than others (Glatzmaier *et al*. 1999). Thus, there is some reason to suppose that analysis of the reversals of the tomographic simulation could have a bearing on the question of preferred bands, even though the conditions assumed for the tomographic simulation must depart substantially from those of the Earth.

To check for VGP preference in the tomographic simulation, we calculated the density of VGPs that would be recorded by sites distributed evenly all over the globe at all the time-steps in an interval that is twice as long as, and centred on, each polarity transition. Figure 16*a* shows a map of the results for the first tomographic reversal. The highest density areas of transitional VGPs straddle the Equator around 270° E longitude. They are part of a broad swath that extends over the Americas

Downloaded from rsta.royalsocietypublishing.org

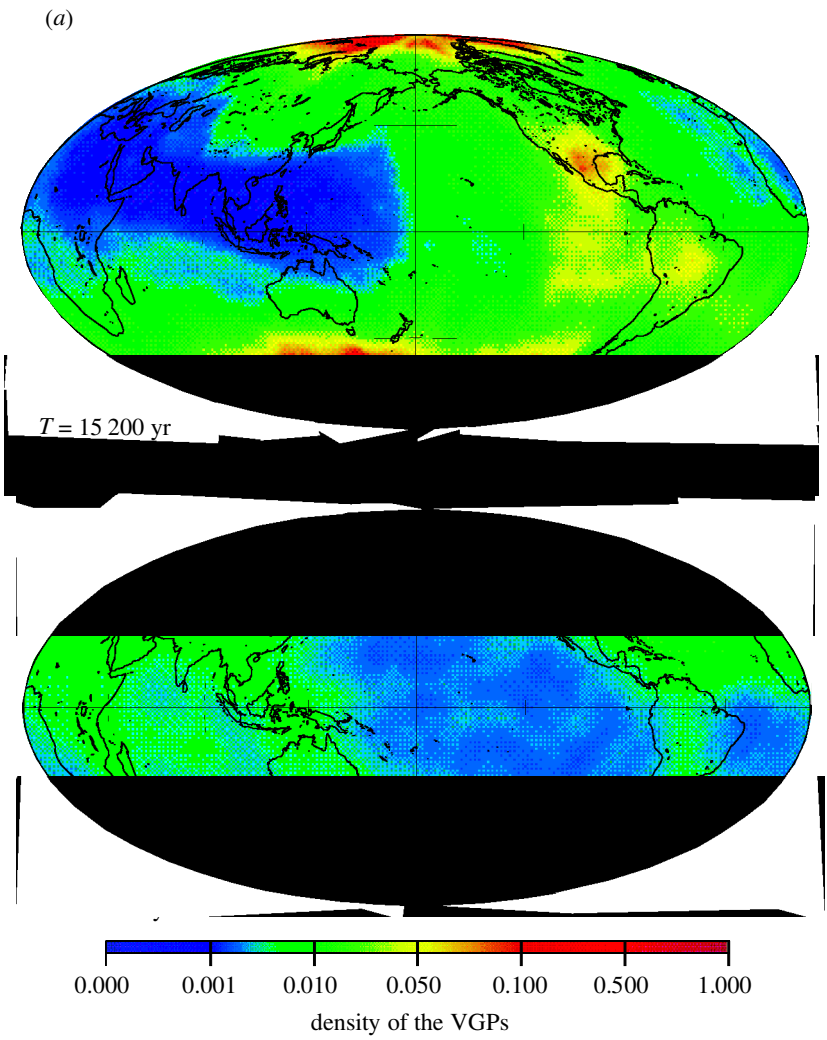

Figure 16. VGP density for time-intervals spanning the first tomographic reversal (a) and the second tomographic reversal (b). Note that the colour scale is nonlinear.

and into the Pacific and Atlantic Oceans, but the average density of the swath is much reduced relative to the highest-density, low-latitude areas (note that the colour scale is nonlinear). There is also a hint of higher density over Siberia. The histogram in figure 17a shows the concentration of VGPs more quantitatively. There is a sharp peak centred on 260° E longitude that rises more than a factor of two above the background, and a poorly defined small peak centred on 100° E. In this histogram, a cut-off for VGPs with latitudes higher than 65° has been incorporated to exclude full polarity poles. Choosing a 45° cut-off enhances the main peak to four times above background and all but eliminates the subsidiary peak.

The peak in VGP density centred on 260° E is consistent with the transition pole path for the true dipole field (figure 8c). Further analysis confirms that the clustering of VGPs is due far more to the equatorial dipole than to the non-dipole field, even

Downloaded from rsta.royalsocietypublishing.org

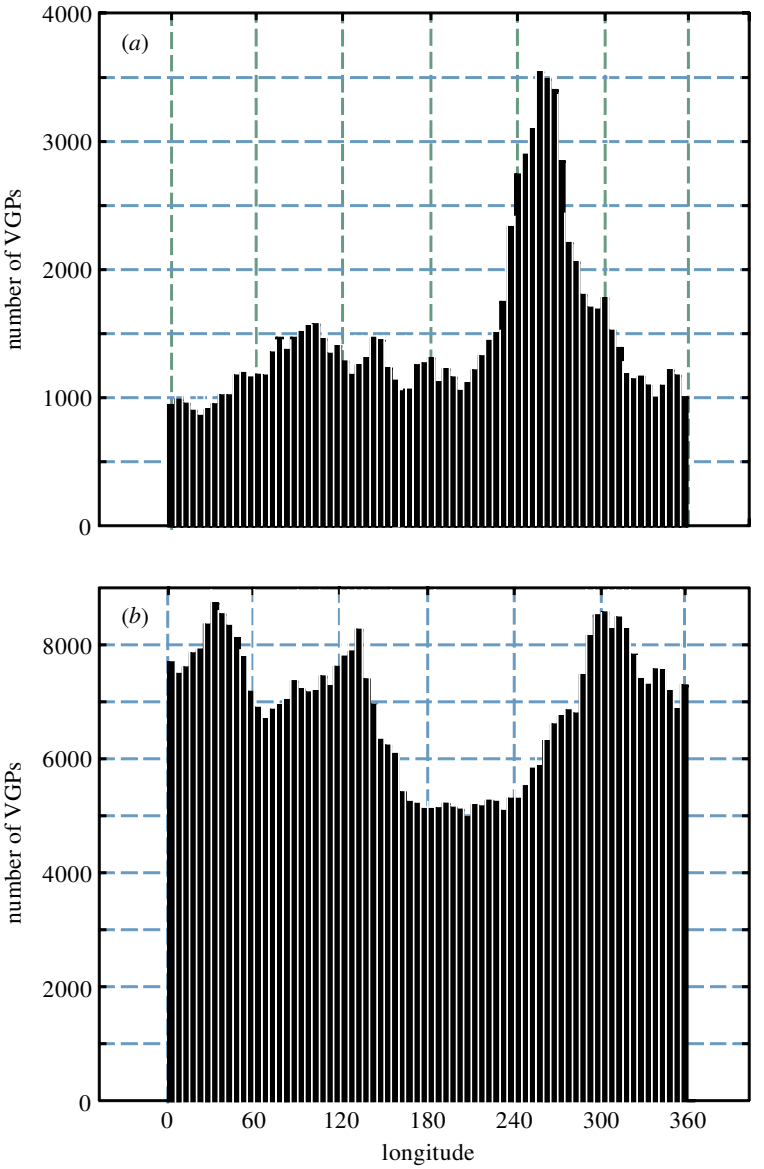

Figure 17. Histograms showing number of VGPs lying in 5° longitude intervals between latitudes of 65° S and 65° N for the tomographic simulation first reversal (*a*) and second reversal (*b*), corresponding to the two VGP density maps in figure 16.

though the latter outweighs the former during much of the transition. Features such as the large positive flux patch at the Equator shown in figure 13*b* have a substantial (1,1) harmonic component that concentrates the VGPs in that longitude band.

The VGP density map for the second tomographic reversal, which is much longer and more complex than the first, reveals a conspicuous absence of transitional poles in the Pacific Basin, a broad smear of poles everywhere else in the Northern Hemisphere, and longitudinal bands of poles over South America, Australia and South Africa

PHILOSOPHICAL TRANSACTIONS OF THE ROYAL SOCIETY A MATHEMATICAL, PHYSICAL & ENGINEERING SCIENCES
PHILOSOPHICAL TRANSACTIONS OF THE ROYAL SOCIETY A MATHEMATICAL, PHYSICAL & ENGINEERING SCIENCES

Downloaded from rsta.royalsocietypublishing.org

PHILOSOPHICAL TRANSACTIONS OF THE ROYAL SOCIETY A MATHEMATICAL, PHYSICAL & ENGINEERING SCIENCES

(figure 16*b*). The histogram in figure 17*b* confirms this impression. There are three distinct peaks in VGP density at 30, 130 and 300° E longitude corresponding to these bands and a deep minimum across the Pacific. The peaks, however, only rise 15% above the troughs that separate them, except for the broad Pacific trough, in which they stand 70% above. Choosing a 45° latitudinal cut-off enhances the depth of the Pacific trough significantly, but reduces the Australian peak to a shoulder on the African peak, and only slightly sharpens the distinction between the American and African peaks. Again, further analysis shows that the distribution of transitional VGPs with longitude resembles that of the true dipole.

These results do correlate broadly with the CMB heat flux pattern imposed in the tomographic simulation (figure 1). The high peak in VGP density at 270° E in the first reversal corresponds well to the top of the elongate heat flux maximum under the Americas. The VGP density peaks of the second reversal, however, are on the flanks of the positive heat flux features, while the VGP density low corresponds to the CMB heat flux low under the Pacific, but also overlaps the western half of the heat flux high under South America. Superimposing the VGP densities from both simulations fits the heat flux pattern somewhat better, especially the broad high from East Africa to Central Australia. More reversals are needed to test the robustness of this correspondence. Nonetheless, we can say that the simulations do appear, so far, to offer some support for VGP preference hypotheses.

5. Conclusions

Both the homogeneous and tomographic simulations have run for *ca.* 300 kyr, and both have reversed polarity twice. This is comparable with the average reversal rate of the recent geomagnetic field, which is one every 200–250 kyr. Although neither simulation accurately reproduces all the properties of the spatially or temporally averaged geomagnetic field, neither today's field nor the time-averaged field of the past 5 Ma, they are encouragingly earth-like in their spatial power spectra. In terms of temporal variability, the homogeneous simulation displays on average somewhat less and the tomographic simulation somewhat more secular variation than the Earth.

The two homogeneous reversals and the first tomographic reversal fit the stereotype inferred from palaeomagnetic recordings of real reversals rather well: duration 2–10 kyr, low dipole intensity during the transition, and VGP paths that usually cross the Equator quickly and are adorned with excursions and rebounds. Locally, however, the first tomographic reversal exhibited unusually large field intensities in the early stages of the transition and at its close. These arose from flux patches that suddenly sprang into existence and quickly became very intense. The second tomographic reversal is quite different, consisting of a progressive collapse of the dipole intensity, a protracted period (22 kyr) of polarity change marked by repeated large oscillations in direction, and an extremely slow recovery of dipole intensity. It raises the question of whether such a long and complex polarity transition has never been observed palaeomagnetically, or just never reported.

The reversals are quite different in spatial variability of magnetic signature and the extent to which they are time transgressive, that is, the extent to which the reversal happens earlier or later at different places around the globe. The two homogeneous reversals are simple, so that at most localities the VGP crosses the Equator only once and the midpoint of the transition is well defined. For the first, this point occurs

Downloaded from rsta.royalsocietypublishing.org

PHILOSOPHICAL TRANSACTIONS OF THE ROYAL SOCIETY A MATHEMATICAL, PHYSICAL & ENGINEERING SCIENCES

initially in a limited range of longitudes at the Equator and finally at high southerly latitudes, almost 2000 years later. For the second it varies by 800 years around the globe. The first tomographic reversal is more complex, but its time transgression can also be estimated reasonably well at 2000 years. The last tomographic reversal is so complex that it is necessary to mark the first and last times the VGP crosses the Equator. By this measure, the time transgression at the beginning is 11 kyr between the north and south polar regions and 3 kyr at the end, and the duration of the reversal ranges from 8 kyr in the north to 22 kyr in the south.

The simulations are chaotic, and the reversals occur spontaneously and are so different that there is probably no specific trigger that sets them off. Nonetheless, all of the reversals started during an upward trend in the time-averaged non-dipole field energy density. In the second homogeneous and first tomographic reversals we see a large, abrupt increase in non-dipole energy that coincides with a decrease in dipole energy and leads quickly to a further decrease in the dipole and reversal of polarity. This behaviour strongly reminds one of the early ideas of Cox (1968). Furthermore, each homogeneous reversal occurs after a long-term decrease in the dipole energy as it nears an apparent threshold at $10^8\ \mathrm{nT}^2$, and after the polarity change the energy builds back up to a significantly higher value than it had just before. This gives the intensity records a sawtooth appearance, much like that observed by Valet & Meynadier (1993) in their study of relative palaeointensity in marine sediments.

The four reversals also differ significantly in transitional field morphology. The first and second homogeneous reversals are dominantly non-dipolar, that is, the non-dipole energy is higher than the equatorial dipole energy when the axial dipole is very weak. The major Gauss components in the first transition belong to the anti-symmetric group and in the second to the symmetric group. The first tomographic reversal is dominated by the equatorial dipole in the middle of the transition and by a mixture of quadrupolar components at the beginning and end, giving it an overall symmetric transition field. The second, long reversal of the tomographic simulation has no well-defined middle. Its succession of many different Gauss components that contribute to the transition field definitely make it mixed in character, but overall it has a non-dipolar and symmetric flavour. In summary, there is no strong rule as to the dominant character of the transition fields in these simulations, although symmetric, non-dipolar fields are more prevalent so far. The strongest conclusion of this entire analysis is that each reversal in the simulations has its own unique character, which can differ greatly in various aspects from others. The same may well be true for the Earth.

Finally, the densities of transitional VGPs from sites all over the globe exhibit a statistical correlation with areas of higher-than-average CMB heat flux. Both tomographic reversals give a peak in number of VGPs between 260 and 310° E longitude and a broad low in the Pacific region. There is also an indication of a weak high somewhere between 30 and 130° E. The correlation between transitional VGP density and CMB heat flux is crude and requires testing with more reversals, but the simulations do currently appear to offer some support for VGP preference hypotheses.

Support for this research was provided by grants 713A from the Institute of Geophysics and Planetary Physics at Los Alamos National Laboratory, and EAR-9903194 from the National Science Foundation. We thank Jeff Love for his critical review of this paper and Paul Wessel and Walter Smith for the use of GMT software (Wessel & Smith 1995).

Downloaded from rsta.royalsocietypublishing.org

PHILOSOPHICAL TRANSACTIONS OF THE ROYAL SOCIETY A MATHEMATICAL, PHYSICAL & ENGINEERING SCIENCES

References

Bloxham, J. & Gubbins, D. 1987 Thermal core–mantle interactions. *Nature* **325**, 511–513.

Bogue, S. W. & Coe, R. S. 1982 Successive paleomagnetic reversal records from Kauai. *Nature* **295**, 399–401.

Bogue, S. W. & Merrill, R. T. 1992 The character of the field during geomagnetic reversals. *A. Rev. Earth Planet. Sci.* **20**, 181–219.

Clement, B. M. 1991 Geographical distribution of transitional VGPs: evidence for non-zonal equatorial symmetry during the Matuyama–Brunhes geomagnetic reversal. *Earth Planet. Sci. Lett.* **104**, 48–58.

Clement, B. M. 1992 Evidence for dipolar fields during the Cobb Mountain geomagnetic polarity reversals. *Nature* **358**, 405.

Clement, B. M. & Kent, D. V. 1984 Latitudinal dependency of geomagnetic polarity transition durations. *Nature* **310**, 488–491.

Clement, B. M. & Kent, D. V. 1991 A southern hemisphere record of the Matuyama–Brunhes polarity reversal. *Geophys. Res. Lett.* **18**, 81–84.

Clement, B. M., Rodda, P., Smith, E. & Sierra, L. 1995 Recurring transitional geomagnetic field geometries: evidence from sediments and lavas. *Geophys. Res. Lett.* **22**, 3171–3174.

Cox, A. 1968 Lengths of geomagnetic polarity intervals. *J. Geophys. Res.* **73**, 3249–3260.

Cox, A. & Doell, R. R. 1964 Long period variations of the geomagnetic field. *Bull. Seism. Soc. Am.* **54**, 2243–2270.

Creer, K. M. & Ispir, Y. 1970 An interpretation of the behavior of the geomagnetic field during polarity transitions. *Phys. Earth. Planet. Interiors* **2**, 115–127.

Fuller, M. D., Williams, I. & Hoffman, K. A. 1979 Paleomagnetic records of geomagnetic field reversals and the morphology of the transitional fields. *Rev. Geophys. Space Phys.* **17**, 179–203.

Glass, B. P. & Heezen, B. C. 1967 Tektites and geomagnetic reversals. *Sci. Am.* **217**, 32.

Glatzmaier, G. A. & Roberts, P. H. 1996 An anelastic evolutionary geodynamo simulation driven by compositional and thermal convection. *Physica* D **97**, 81–94.

Glatzmaier, G. A. & Roberts, P. H. 1997 Simulating the geodynamo. *Contemp. Phys.* **38**, 269–288.

Glatzmaier, G. A., Coe, R. S., Hongre, L. & Roberts, P. H. 1999 The role of the Earth's mantle in controlling the frequency of geomagnetic reversals. *Nature* **401**, 885–890.

Glen, J. M., Coe, R. S. & Liddicoat, J. C. 1994 Persistent features of polarity transition records from western North America. *Geophys. Res. Lett.* **21**, 1165–1168.

Glen, J. M., Coe, R. S. & Liddicoat, J. C. 1999 A detailed record of paleomagnetic field change from Searles Lake, California. 2. The Gauss/Matuyama polarity reversal. *J. Geophys. Res.* **104**, 12 883–12 894.

Gubbins, D. 1994 Geomagnetic polarity reversals: a connection with secular variation and core–mantle interaction? *Rev. Geophys. Space Phys.* **32**, 61–83.

Gubbins, D. & Coe, R. S. 1993 Longitudinally confined geomagnetic reversal paths from nondipole transition fields. *Nature* **362**, 51–53.

Guyodo, Y. & Valet, J.-P. 1999 Global changes in intensity of the Earth's magnetic field during the past 800 kyr. *Nature* **399**, 249–252.

Heirtzler, J. R. 1970 The palaeomagnetic field as inferred from marine magnetic studies. *J. Geomag. Geoelect.* **22**, 197.

Herrero-Bervera, E. & Coe, R. S. 1999 Transitional field behavior during the Gilbert–Gauss and Lower Mammoth reversals recorded in lavas from the Waianae Volcano, O'ahu, Hawaii. *J. Geophys. Res.* **104**, 29 157–29 173.

Downloaded from rsta.royalsocietypublishing.org

PHILOSOPHICAL TRANSACTIONS OF THE ROYAL SOCIETY A MATHEMATICAL, PHYSICAL & ENGINEERING SCIENCES

Herrero-Bervera, E. & Theyer, F. 1986 Non-axisymmetric behaviour of Olduvai and Jaramillo polarity transitions recorded in north-central Pacific deep-sea sediments. *Nature* **322**, 159–162.

Herrero-Bervera, E., Theyer, F. & Helsley, C. E. 1987 Olduvai onset polarity transition: two detailed palaeomagnetic records from North Central Pacific sediments. *Phys. Earth Planet. Interiors* **49**, 325.

Hide, R. 1970 On the Earth's core–mantle interface. *Q. J. R. Meteorol. Soc.* **96**, 579–590.

Hillhouse, J. & Cox, A. 1976 Brunhes–Matuyama polarity transition. *Earth Planet. Sci. Lett.* **29**, 51–64.

Hoffman, K. A. 1977 Polarity transition records and the geomagnetic dynamo. *Science* **196**, 1329–1332.

Hoffman, K. A. 1979 Behavior of the geodynamo during reversal: a phenomenological model. *Earth Planet. Sci. Lett.* **44**, 7–17.

Hoffman, K. A. 1992 Dipolar reversal states of the geomagnetic field and core–mantle dynamics. *Nature* **359**, 789–794.

Hoffman, K. A. 1996 Transitional paleomagnetic field behavior: preferred paths or patches? *Surv. Geophys.* **17**, 207–211.

Hongre, L., Hulot, G. & Khokhlov, A. 1998 An analysis of the geomagnetic field over the past 2000 years. *Phys. Earth Planet. Interiors* **106**, 311–335.

Jacobs, J. A. 1994 *Reversals of Earth's magnetic field*. Cambridge University Press.

Johnson, C. & Constable, C. 1995 The time-averaged field as recorded by lava flows over the past 5 Myr. *Geophys. J. Int.* **122**, 489–519.

Juarez, M. T., Tauxe, L., Gee, J. S. & Pick, T. 1998 The intensity of the Earth's magnetic field over the past 160 million years. *Nature* **394**, 878–881.

Laj, C., Mazaud, A., Weeks, R., Fuller, M. & Herrero-Bervera, E. 1991 Geomagnetic reversal paths. *Nature* **351**, 447.

Langel, R. A. & Estes, R. H. 1982 A geomagnetic field spectrum. *Geophys. Res. Lett.* **9**, 250–253.

Langereis, C. G., van Hoof, A. A. M. & Rochette, P. 1992 Longitudinal confinement of geomagnetic reversal paths as a possible sedimentary artefact. *Nature* **358**, 226–230.

Lay, T., Williams, Q. & Garnero, E. 1998 The core–mantle boundary and deep earth dynamics. *Nature* **392**, 461–468.

Love, J. J. 1998 Paleomagnetic volcanic data and geometric regularity of reversals and excursions. *J. Geophys. Res.* **103**, 12 435–12 452.

Lowes, F. J. 1974 Spatial power spectrum of the main geomagnetic field, and extrapolation to the core. *Geophys. J. R. Astr. Soc.* **36**, 717–730.

McElhinny, M. W., McFadden, P. L. & Merrill, R. T. 1996 The time-averaged field 0–5 Ma. *J. Geophys. Res.* **101**, 25 007–25 027.

McFadden, P. L. & Merrill, R. T. 1986 Geodynamo energy source constraints from paleomagnetic data. *Phys. Earth Planet. Interiors* **43**, 22–33.

McFadden, P. L., Merrill, R. T., McElhinny, M. W. & Lee, S. 1991 Reversals of the Earth's magnetic field and temporal variations of the dynamo families. *J. Geophys. Res.* **96**, 3923–3933.

McFadden, P. L., Merrill, R. T. & Barton, C. E. 1993 Do virtual geomagnetic poles follow preferred paths during geomagnetic reversals? *Nature* **361**, 342–344.

Mankinen, E. A., Prévot, M., Grommé, C. S. & Coe, R. S. 1985 The Steens Mountain (Oregon) geomagnetic polarity transition. 1. Directional history, duration of eipisodes, and rock magnetism. *J. Geophys. Res.* **90**, 10 393–10 416.

Merrill, R. T. & McFadden, P. L. 1990 Paleomagnetism and the nature of the geodynamo. *Science* **248**, 345–350.

Merrill, R. T., McElhinny, M. W. & McFadden, P. L. 1996 *The magnetic field of the Earth: paleomagnetism, the core, and the deep mantle*. Academic.

Downloaded from rsta.royalsocietypublishing.org

Momose, K. 1963 Studies on the variations of the Earth's magnetic field during Pliocene times. *Bull. Earthq. Res. Inst.* **41**, 487–534.

Muller, R. & Morris, D. 1986 Geomagnetic reversals from impacts on the Earth. *Geophys. Res. Lett.* **13**, 1177.

Niitsuma, N. 1971 Paleomagnetic and paleoenvironmental study of sediments recording the Matuyama–Brunhes geomagnetic reversal. *Tohoku Univ. Sci. Rep. Second Ser. (Geology)* **43**, 1–39.

Prévot, M. & Camps, P. 1993 Absence of preferred longitudinal sectors for poles from volcanic records of geomagnetic reversals. *Nature* **366**, 53–57.

Prévot, M., Mankinen, E. A., Coe, R. S. & Grommé, C. S. 1985*a* How the geomagnetic field vector reverses polarity. *Nature* **316**, 230.

Prévot, M., Mankinen, E. A., Coe, R. S. & Grommé, C. S. 1985*b* The Steens Mountain (Oregon) geomagnetic polarity transition. 2. Field intensity and discussion of reversal models. *J. Geophys. Res.* **90**, 10 417–10 448.

Quidelleur, X. & Valet, J.-P. 1994 Paleomagnetic records of excursions and reversals: possible biases caused by magnetization artefacts. *Phys. Earth Planet. Interiors* **82**, 27–48.

Quidelleur, X., Valet, J.-P., LeGoff, M. & Bouldoire, X. 1995 Field dependence on magnetization of laboratory-redeposited deep-sea sediments: first results. *Earth Planet. Sci. Lett.* **133**, 311–325.

Rochette, P. 1990 Rationale of geomagnetic reversals versus remanence recording processes: a critical review. *Earth Planet. Sci. Lett.* **98**, 33–39.

Steinhauser, P. & Vincenz, S. A. 1973 Equatorial paleopoles and behavior of the dipole field during polarity transitions. *Earth Planet. Sci. Lett.* **19**, 113–119.

Su, W.-J., Woodward, R. L. & Dziewonski, A. N. 1994 Degree-12 model of shear velocity heterogeneity in the mantle. *J. Geophys. Res.* **99**, 6945–6980.

Tackley, P. J., Stevenson, D. J., Glatzmaier, G. A. & Schubert, G. 1994 Effects of multiple phase transitions in a 3-D spherical model of convection in the Earth's mantle. *J. Geophys. Res.* **99**, 15 877–15 901.

Tric, E., Laj, C., Jehanno, C., Valet, J.-P., Kissel, C., Mazaud, A. & Iaccarino, S. 1991 High-resolution record of the upper Olduvai transition from Po Valley (Italy) sediments; support for dipolar transition geometry? *Phys. Earth Planet. Sci. Lett.* **65**, 319–336.

Valet, J.-P. & Meynadier, L. 1993 Geomagnetic field intensity and reversals during the past four million years. *Nature* **366**, 234–238.

Valet, J.-P., Tauxe, L. & Clark, D. 1988 The Matuyama–Brunhes transition recorded in Lake Tecopa sediments (California). *Earth Planet. Sci. Lett.* **87**, 463–472.

Valet, J.-P., Tucholka, P., Courtillot, V. & Meynadier, L. 1992 Palaeomagnetic constraints on the geometry of the geomagnetic field during reversals. *Nature* **356**, 400–407.

Van Zijl, J. S. V., Graham, K. W. T. & Hales, A. L. 1962 The paleomagnetism of the Stormberg lavas. II. The behaviour of the magnetic field during a reversal. *Geophys. J. R. Astr. Soc.* **7**, 169–182.

Wessel, P. & Smith, W. H. F. 1995 New version of the Generic Mapping Tools released. *Eos* **76**, 329.

Williams, I. S. & Fuller, M. 1981 Zonal harmonic models of reversal transition fields. *J. Geophys. Res.* **86**, 11 657–11 665.